

Online-Score-Aided Federated Learning: Taming the Resource Constraints in Wireless Networks

Md Ferdous Pervej, *Member, IEEE*, Minseok Choi, *Member, IEEE*, and Andreas F. Molisch, *Fellow, IEEE*

Abstract—While federated learning (FL) is a widely popular distributed ML strategy that protects data privacy, time-varying wireless network parameters and heterogeneous system configurations of the wireless device pose significant challenges. Although the limited radio and computational resources of the network and the clients, respectively, are widely acknowledged, two critical yet often ignored aspects are (a) wireless devices can only dedicate a small chunk of their limited storage for the FL task and (b) new training samples may arrive in an online manner in many practical wireless applications. Therefore, we propose a new FL algorithm called **online-score-aided federated learning (OSAFL)**, specifically designed to learn tasks relevant to wireless applications under these practical considerations. Since it has long been proven that under extreme resource constraints, clients may perform an arbitrary number of local training steps, which may lead to client drift under statistically heterogeneous data distributions, we leverage normalized gradient similarities and exploit weighting clients' updates based on optimized scores that facilitate the convergence rate of the proposed OSAFL algorithm. Our extensive simulation results on two different tasks—each with three different datasets—with four popular ML models validate the effectiveness of OSAFL compared to six existing state-of-the-art FL baselines.

Index Terms—Federated learning, resource constrained learning, wireless applications, wireless networks.

I. INTRODUCTION

THE widely popular federated learning (FL) [1] is a distributed machine learning (ML) approach that enables training an ML model $\mathbf{w} \in \mathbb{R}^N$ across distributed clients' local datasets. A central server (CS) typically broadcasts the model to $\mathcal{U} = \{u\}_{u=0}^{U-1}$ clients, who then train the received model on their respective local dataset \mathcal{D}_u to minimize the following loss function.

$$f_u(\mathbf{w}|\mathcal{D}_u) := \frac{1}{|\mathcal{D}_u|} \sum_{(\mathbf{x},y) \in \mathcal{D}_u} l(\mathbf{w}|\mathbf{x},y), \quad (1)$$

where $\mathcal{D} := \bigcup_{u=0}^{U-1} \mathcal{D}_u$ and $l(\mathbf{w}|\mathbf{x},y)$ is the loss associated to training sample (\mathbf{x},y) . Moreover, \mathbf{x} and y are the training feature and label, respectively. As such, an FL algorithm is designed to train \mathbf{w} distributively by optimizing the following objective function [1].

$$\underset{\mathbf{w}}{\text{minimize}} \quad f(\mathbf{w}|\mathcal{D}) := \sum_{u=0}^{U-1} \alpha_u f_u(\mathbf{w}|\mathcal{D}_u), \quad (2)$$

where $0 \leq \alpha_u \leq 1$ with $\sum_{u=0}^{U-1} \alpha_u = 1$ and $\mathcal{D} = \bigcup_{u=0}^{U-1} \mathcal{D}_u$. Since a client's loss function $f_u(\mathbf{w}|\mathcal{D}_u)$ depends on its local dataset \mathcal{D}_u and the global loss function $f(\mathbf{w}|\mathcal{D})$ is a weighted combination

of the clients' loss functions, clients' datasets directly impact the global loss function.

While FL in wireless networks is particularly attractive since the clients do not need to offload their privacy-sensitive data to the server, constraints from the client and network sides need to be acknowledged [2]. Besides, one fundamental assumption in typical FL is that the client has a static dataset \mathcal{D}_u , which is readily available before training begins. However, \mathcal{D}_u may not be static and/or readily available in many practical applications [3], [4]. Moreover, the statistical data distributions of the clients may not necessarily remain static. The training samples can arrive in a causal manner [5], [3], [4] in many applications. This is particularly true for many wireless applications, such as integrated sensing and communication (ISAC) [6], temporal/online channel state information (CSI) prediction [7], demand predictions in video caching network [3], etc.

The limited storage sizes of the clients create another major concern in devising an efficient FL solution in wireless networks. In particular, owing to the limited storage, clients can only store a limited number of training samples. Client devices are not solely expected to store these training samples and the ML model: these devices also store different files that are generated/saved by the users and operational files for the operating system (OS). Therefore, only a small chunk of the limited storage can be used for the FL task. This can exacerbate the learning process, especially when the clients have very limited storage, e.g., Internet of Things (IoT) devices. As such, when new training samples arrive, clients may need to remove old samples to make space for the newly arrived samples. Therefore, the deleted samples will be lost forever.

A time-varying dataset and ephemeral utilization of some training samples can lead to severe performance degradation compared to general model training with a stationary dataset that seeks to minimize the loss function in (1). Under data scarcity, some changes in the client's dataset \mathcal{D}_u during a training round may shift the statistical data distribution and the local optimizer's trajectory, creating instability in the prediction performance. For example, Fig. 1 shows the performance comparisons of the traditional centralized mini-batch stochastic gradient descent (SGD) algorithm [8] on the popular CIFAR-10 dataset [9]. The empirical performance explicitly points out the performance deviations and instability when \mathcal{D}_u changes over time. Therefore, when \mathcal{D}_u can change over training time, we need to pay special attention and customize the learning algorithms. Besides, since the existing FL algorithms mainly considered static datasets, those may perform poorly in such practical resource-constrained cases. As such, any change in training datasets due to new sample arrival and old sample departure to accommodate the fixed

This work was supported by NSF-IITP Project 2152646.

Md Ferdous Pervej and Andreas F. Molisch are with the Ming Hsieh Department of Electrical and Computer Engineering, University of Southern California, Los Angeles, CA 90089 USA (e-mail: pervej@usc.edu; molisch@usc.edu).

Minseok Choi is with the Department of Electronic Engineering, Kyung Hee University, Republic of South Korea (email: choisms@khu.ac.kr)

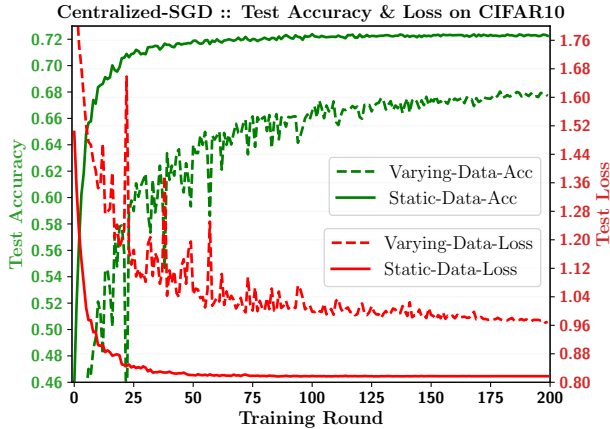


Fig. 1: Static vs. time varying datasets: test metrics comparisons on CIFAR-10 dataset [9]

memory storage of the clients necessitates new theoretical analysis and new FL learning algorithms. Moreover, depending on the ML model size, some clients may only store a few training samples, and training the model on these few initial samples may not sufficiently capture the data distribution change that can exacerbate the test performance.

A. State-of-the-Art FL Algorithms

The so-called federated averaging (FedAvg) algorithm [1] paved the way for privacy-preserving FL. This seminal work considers that distributed clients train a global model in their local datasets for an equal number of local rounds and offload the trained model parameters to the central server. However, this is not practical in many cases where system heterogeneity can introduce stragglers. Besides, under non-IID (independent and identically distributed) data distribution, client u 's \mathcal{D}_u statistically differ from client u' 's $\mathcal{D}_{u'}$ which introduces client-drift in FedAvg [10].

Following FedAvg, many works [11], [10], [12], [13], [14] were proposed to address the issues of system and data heterogeneity. FedProx [11] was proposed to mitigate the straggler effect by allowing partially locally trained model aggregation, and a proximal term was added to the local objective function in order to keep the local model parameter close to the initially received global model. Karimireddy *et al.* [10] also exploited a similar idea. In this work, the authors proposed stochastic controlled averaging algorithm (SCAFFOLD) that mitigates client drifts using local control variates. More specifically, in order to control the drift, a correctional variate is added to the client's updated gradient to find the updated local model. The problem of system heterogeneity was further explored in federated normalized averaging (FedNova) [12]. In this pioneering work, the authors advocated aggregating clients' normalized trained gradients instead of using their raw trained gradients to find the global model. Yang *et al.* also adopted the normalized gradients aggregation policy and partial client participation in their proposed algorithm called anarchic federated averaging (AFA) [13] to handle the data and system heterogeneity. Moreover, recently, Ye *et al.* proposed federated learning with discrepancy-aware collaboration

(FedDisco) that takes label/class distribution discrepancies into account in model aggregation weights [14]. The authors find sub-optimal aggregation weights that explicitly consider these discrepancies.

B. State-of-the-art FL in Wireless Networks

There are a plethora of recent studies [15], [16], [17], [18], [19] that customize the above general FL algorithms and train them in wireless networks. Most noticeably, the intertwined wireless networking and FL parameters are often optimized jointly when the ML model is exchanged between the clients and CS using the time-varying wireless fading channels between the clients and base station (BS)¹ [15], [16], [17], [18], [19]. Some slight variations of the above studies also exist. Zhao *et al.* proposed a model-ensemble-based FL framework where clients with similar data distributions are kept in a cluster, and each such cluster acts as a parameter server to train a cluster model using the associated clients [20]. During the training phase, the clusters train their respective models without any global aggregation. However, an ensemble model is generated from the trained cluster models during the inference phase. It is also common to allocate resources to facilitate FL in wireless networks [21], [22]. Clients' transmit powers can be optimized to maximize signal-to-interference-plus-noise ratio to ensure model parameters are received at the BS [21]. Besides, resource costs for model training and benefits from such training—in terms of model accuracy—can be assessed in order to proportionately allocate network and computing resources to achieve a certain level of accuracy [22].

Due to practical resource constraints in wireless networks and on the client side, all clients may not participate in model training in every global round, which motivates partial client selection for model training [3], [23], [24], [25], [26]. In our earlier work [3], we proposed a resource-aware hierarchical federated learning (HFL) with partial client participation, where clients were selected to optimize a weighted objective function that strikes a balance between the number of local SGD steps and the corresponding energy expense. Zhang *et al.* proposed a FedAvg-based algorithm where a heuristic method was proposed for jointly configuring client scheduling, client's local training rounds and radio resource allocations in wireless networks [23]. Saha *et al.* quantified data quality by data volume and label heterogeneity and then leveraged the data quality to select subset clients for model training [24]. Yao *et al.* also optimized partial client participation [25]. In particular, the authors proposed using the updated local model of the clients and the reuse of the previous round's global model instead for the global model update policy when the uplink transmissions from the clients are error-free and erroneous, respectively. Recently, Chen *et al.* not only considered partial client selection for FL in resource-constrained wireless networks, but also proposed partial model aggregations - only a few layers of the entire model are exchanged and aggregated [26].

¹These studies assume the BS acts as the CS or the BS works as the medium to transport the model parameters between the clients and CS.

Model pruning [27] and quantization [28] are the other two prominent avenues to alleviate clients' limited computational power and communication overheads. While model pruning and model quantization are intended to mitigate resource constraints and leverage similar ideas, they differ largely in theory. In model pruning, some of the neurons of the ML models are pruned to reduce the training overhead. In contrast, all parameters are quantized in model quantization, and the training happens with the quantized parameters. Naturally, some recent works [29], [30], [31], [32] utilized these concepts for performing FL in wireless networks. In particular, [29], [30] propose leveraging model pruning and optimizing the pruning ratio based on available resources at the client and network sides. Besides, [31] and [32] advocate choosing the quantization levels according to the available wireless and computation resources.

C. Research Gaps and Our Contributions

The above studies established how system heterogeneity and constrained wireless network resources necessitate jointly optimizing the resources from the client and network sides. One fundamental parameter is how many local training steps a client can perform before it needs to send the trained model to the CS. Based on available resources and network conditions, this number can differ significantly. However, the above studies still consider static datasets, assuming all training data are readily available. This is certainly not the case in many practical systems that have clients with very limited storage capacities. This mandates proper data management and modified algorithms to capture the impact of the ephemeral training samples on the trained model parameters. In this paper, we, therefore, propose an online-score-aided federated learning (OSAFL) algorithm to address these shortcomings. Our key contributions are summarized below.

- We design a new algorithm—called OSAFL—that especially considers time-varying and resource-constrained characteristics of the underlying wireless networks and the clients, assuming that the clients perform an arbitrary number of local training steps and design old training sample removal procedures to tame the non-IID label distributions in classification tasks.
- In order to handle the system and data heterogeneity, we utilize the normalized trained gradients in global model aggregation policy and also leverage gradient similarity as a measure to capture the impact of the ephemeral training samples on the local gradient. More specifically, the CS optimizes weighting factors based on the theoretical convergence analysis of OSAFL that depends on the gradient similarities to update its global model.
- Through extensive simulations, we validate the performance of the proposed OSAFL algorithm on two different tasks - each consisting of three datasets, using four popular ML models and six state-of-the-art FL baselines.

The rest of the paper is organized as follows. We first introduce our OSAFL algorithm in Section II. Then, we conduct an extensive theoretical analysis of the proposed algorithm in Section III, followed by our empirical analysis

and discussions in Section IV. Finally, Section V concludes the paper.

II. ONLINE-SCORE-AIDED FL FOR WIRELESS APPLICATIONS

In this work, we consider that wireless devices act as clients, and the CS is embedded into the clients' serving BS.

A. FL with Time-Varying Dataset: Preliminaries

1) *Dataset Acquisition for Model Training*: Since the wireless devices have limited resources, we assume that each client has a limited storage that can be dedicated to store the ML model and the training samples. Without any loss of generality, denote the maximum number of training data samples that client u can store by D_u . Besides, we assume that each client has its own initial dataset $\mathcal{D}_u^{t=0}$, where $|\mathcal{D}_u^t| = D_u$, $|\cdot|$ represents the cardinality of a set and t represents the t^{th} FL round. Furthermore, we consider that each client can have at most E_u new training samples between two consecutive FL rounds. It is worth noting that the newly arrived samples follow the same parameters as in the initial non-IID distributions of the clients². We interpret this as E_u possible sample arrival slots between two FL rounds. In each of these arrival slots, the new sample arrival is modeled as an independent *Bernoulli* distribution with *success probability* $p_{u,ac}$. As such, the total number of new training samples between two FL rounds can be modeled as a *Binomial* distribution with parameters $(E_u, p_{u,ac})$.

As each client can only store D_u training samples, when a new training sample arrives, the client must remove an old training sample to make space for the newly arrived sample. This removal process can follow different techniques. For example, a simple approach is removing the oldest training sample in the dataset following a *first-in-first-out* (FIFO) policy. Another approach can be removing the oldest sample from the top-most class. We call this method *trim top label* (TrimTopLabel), which could help us to tame the label distribution skewness, especially when the clients have severe non-IID data distribution. Moreover, other policies can also be incorporated easily. It is worth noting that we consider E to be relatively small, and the dataset is only updated before the start of a new global round. In practice, the arrived sample can be held in a temporary buffer, and the dataset can be updated only once before a new global round starts. Therefore, the training dataset \mathcal{D}_u^t remains unchanged until the next, i.e., $(t+1)^{\text{th}}$ FL round begins.

2) *FL with Time Varying Datasets*: Let us denote the global model during global round t by \mathbf{w}^t . Since dataset \mathcal{D}_u^t is dynamic, with the FedAvg algorithm [1], the CS aims to minimize the following objective function in each FL round.

$$f(\mathbf{w}^t | \mathcal{D}^t) := \sum_{u=0}^{U-1} \alpha_u f_u(\mathbf{w}^t | \mathcal{D}_u^t), \quad (3)$$

where $\mathcal{D}^t := \bigcup_{u=0}^{U-1} \mathcal{D}_u^t$ and $f_u(\mathbf{w} | \mathcal{D}_u^t)$ is the local objective function of client u , which is defined as

$$f_u(\mathbf{w} | \mathcal{D}_u^t) := (1/|\mathcal{D}_u^t|) \sum_{(\mathbf{x}, y) \in \mathcal{D}_u^t} l(\mathbf{w} | (\mathbf{x}, y)). \quad (4)$$

²Even though the distribution parameters are the same, the instantaneous label/data distribution can still vary in each round t since these new samples are some realizations of the random distributions.

Notice that the local and global objective functions with the dynamic datasets differ from the objective function in the general static case, as shown in (1) and (2), respectively.

B. Proposed Online-Score-Aided FL (OSAFL) Algorithm

When the client's dataset \mathcal{D}_u^t is dynamic, a mere modification of the global objective function (3) may not be sufficient to capture the intricate impact of the ephemeral training samples in the global model's performance. As such, we present our proposed OSAFL algorithm in what follows.

1) *Online-Score-Aided FL (OSAFL) Algorithm:* At the beginning of each global round, each client receives the updated global model \mathbf{w}^t from the CS and synchronizes the local model as

$$\mathbf{w}_u^{t,0} \leftarrow \mathbf{w}^t, \quad (5)$$

The clients then perform $\kappa_u^t \in \mathbb{Z}^+$ local SGD steps on their local datasets to minimize (4) and update their models as

$$\mathbf{w}_u^{t,\kappa_u^t} = \mathbf{w}_u^{t,0} - \eta \sum_{\tau=0}^{\kappa_u^t-1} g_u(\mathbf{w}_u^{t,\tau} | \mathcal{D}_u^t), \quad (6)$$

where $g_u(\mathbf{w}_u^{t,\tau} | \mathcal{D}_u^t)$ is the unbiased stochastic gradient of client u and η is the local learning rate. Note that the number of local SGD steps shall depend on the clients' available computational resources and the required time to upload the trained model, which largely depends on the wireless network condition. In practice, this is often optimized jointly with other configuration parameters in wireless networks (e.g., see [18], [30], [3] and the references therein). As such, we keep our algorithm general and assume that each client chooses κ_u^t uniformly randomly from $[1, \kappa]$ to imitate such randomness.

Once the clients finish their local training, they calculate the normalized accumulated gradients as

$$\mathbf{d}_u^t := \frac{1}{\kappa_u^t} \sum_{\tau=0}^{\kappa_u^t-1} g_u(\mathbf{w}_u^{t,\tau} | \mathcal{D}_u^t) = \frac{\mathbf{w}_u^{t,0} - \mathbf{w}_u^{t,\kappa_u^t}}{\eta \kappa_u^t}. \quad (7)$$

Each client then sends its \mathbf{d}_u^t to the CS. It is worth noting that normalized gradient is widely used during the global model aggregation instead of the original gradient in the presence of system and data heterogeneity (e.g., see [12], [13], [14], [4] and the references therein).

Upon receiving the updates from the clients, the central server takes a global SGD step with a learning rate of $\tilde{\eta}$ and updates the global model as

$$\mathbf{w}^{t+1} = \mathbf{w}^t - \tilde{\eta} \eta \sum_{u=0}^{U-1} \alpha_u \Delta_u^t \mathbf{d}_u^t = \mathbf{w}^t - \tilde{\eta} \eta \sum_{u=0}^{U-1} \alpha_u \tilde{\mathbf{d}}_u^t, \quad (8)$$

where $\tilde{\mathbf{d}}_u^t := \Delta_u^t \mathbf{d}_u^t$ and $\Delta_u^t \geq 0$ is a weighting factor that we call *score* of client u during round t . This *score* calculation is a general strategy that shall depend on the theoretical analysis and can also be customized for different tasks. Our considered strategy for Δ_u^t is presented in the sequel. Moreover, it is worth noting that OSAFL minimizes the following global objective function.

$$f(\mathbf{w}^t | \mathcal{D}^t) := \sum_{u=0}^{U-1} \alpha_u \Delta_u^t f_u(\mathbf{w}^t | \mathcal{D}_u^t). \quad (9)$$

Therefore, OSAFL seeks a sequence of global models $\mathbf{W}^* = \{\mathbf{w}^{0*}, \mathbf{w}^{1*}, \dots, \mathbf{w}^{T-1*}\}$ so that each \mathbf{w}^{t*} in this sequence minimizes the above global loss function in that global round t .

Algorithm 1 summarizes the key steps of the proposed OSAFL algorithm.

Algorithm 1: Proposed Online-Score-Aided FL

Input: Initial global model \mathbf{w}^0 , client set \mathcal{U} , total global round T , local learning rate η , global learning rate $\tilde{\eta}$

```

1 for  $t = 0$  to  $T - 1$  do
2   for  $u$  in  $\mathcal{U}$  in parallel do
3     Receives the latest global model from the CS
4     Synchronize the local model:  $\mathbf{w}_u^{t,0} \leftarrow \mathbf{w}^t$ 
5     Determine total local SGD steps  $\kappa_u^t \in [1, \kappa]$ 
6     Performs  $\kappa_u^t$  SGD steps:
        $\mathbf{w}_u^{t,\kappa_u^t} = \mathbf{w}_u^{t,0} - \eta \sum_{\tau=0}^{\kappa_u^t-1} g_u(\mathbf{w}_u^{t,\tau})$ 
7     Calculate normalized accumulated gradients
        $\mathbf{d}_u^t := \frac{1}{\kappa_u^t} \sum_{\tau=0}^{\kappa_u^t-1} g_u(\mathbf{w}_u^{t,\tau})$ 
8     Send  $\mathbf{d}_u^t$  to the central server
9   end
10   $\{\Delta_u^t\}_{u=0}^{U-1} \leftarrow \text{Get-Online-Score}(t, \mathbf{d}^t, \{\mathbf{d}_u^t\}_{u=0}^{U-1})$ 
11  Perform global aggregation:  $\mathbf{w}^{t+1} = \mathbf{w}^t - \tilde{\eta} \eta \sum_{u=0}^{U-1} \alpha_u \tilde{\mathbf{d}}_u^t$ 
12 end

```

Output: Trained global model \mathbf{w}^T

2) Gradient Similarities for Online Score Calculations:

As mentioned above and in Algorithm 1, the *score* of the clients plays a critical role in OSAFL. The *score* calculation is modeled as an optimization problem based on the theoretical convergence analysis of the proposed algorithm in the sequel, which considers gradient similarities. Let us define the accumulated normalized gradients at the CS during round t as

$$\mathbf{d}^t := \frac{1}{U} \sum_{u=0}^{U-1} \mathbf{d}_u^t. \quad (10)$$

Then, we calculate the similarity between the individual normalized gradients and the accumulated normalized gradients as follows.

$$\tilde{\lambda}_u^t := \frac{\langle \mathbf{d}^t, \mathbf{d}_u^t \rangle}{\|\mathbf{d}^t\|_2 \cdot \|\mathbf{d}_u^t\|_2}, \quad (11)$$

where $\langle \cdot \rangle$ and $\|\cdot\|$ are the operators to represent the inner product between two vectors and norm of a vector, respectively. Note that $\tilde{\lambda}_u^t$ is essentially the cosine similarity between two vectors and $\tilde{\lambda}_u^t \in [-1, 1]$. Since we consider $\Delta_u^t \geq 0$, we further take the exponent of the cosine similarity as

$$\lambda_u^t := \exp(\tilde{\lambda}_u^t). \quad (12)$$

Remark 1. The score calculation, as well as the gradient similarity calculation, happens in the CS and does not add any additional burden on the clients. The clients only need to offload the normalized gradients, i.e., no additional communication overheads. The calculation of (10) has a time complexity of $\mathcal{O}(N)$. Besides, the inner product calculation in the numerator of (11) has $\mathcal{O}(N)$ complexity, and the L_2 norm calculation has a time complexity of $\mathcal{O}(N)$. Thus, the calculation of $\|\mathbf{d}^t\|_2$ has $\mathcal{O}(N) + \mathcal{O}(1)$ complexity. Furthermore, the denominator of (11) has $\mathcal{O}(N) + \mathcal{O}(1) + \mathcal{O}(N) + \mathcal{O}(1) + \mathcal{O}(1) = \mathcal{O}(N)$ complexity. Therefore, the overall time complexity for getting the exponent of the gradient similarity of a client is $\mathcal{O}(N) + \mathcal{O}(N) + \mathcal{O}(N) + \mathcal{O}(1) = \mathcal{O}(N)$. As such, for all U clients, the CS has a time complexity of $\mathcal{O}(U \times N)$.

III. THEORETICAL ANALYSIS OF OSAFL

We present our detailed theoretical analysis in this section. For brevity and notational simplicity, we represent the local

loss function $f_u(\mathbf{w}|\mathcal{D}_u^t)$ by $f_u(\mathbf{w})$ and the global loss function $f(\mathbf{w}|\mathcal{D})$ by $f(\mathbf{w})$ for the rest of the manuscript. Similarly, the stochastic gradient $g_u(\mathbf{w}|\mathcal{D}_u^t)$ and the true gradient $\nabla f_u(\mathbf{w}|\mathcal{D}_u^t)$ are succinctly denoted by $g_u(\mathbf{w})$ and $\nabla f_u(\mathbf{w})$, respectively. In an FL round t , we should interpret $f_u(\mathbf{w})$ and its gradients $g_u(\mathbf{w})$ and $\nabla f_u(\mathbf{w})$ to be dependent on the client's available dataset \mathcal{D}_u^t , while the global loss function $f(\mathbf{w})$ and its gradient $\nabla f(\mathbf{w})$ depend on \mathcal{D}^t .

A. Assumptions

We make the following standard assumptions [12], [13], [14], [18], [30] that are needed for the theoretical analysis.

Assumption 1 (Smoothness). *The local loss functions are β -Lipschitz smooth. That is, for some $\beta > 0$, $\|\nabla f_u(\mathbf{w}) - \nabla f_u(\mathbf{w}')\| \leq \beta\|\mathbf{w} - \mathbf{w}'\|$, for all $\mathbf{w}, \mathbf{w}' \in \mathbb{R}^N$ and $u \in \mathcal{U}$.*

Assumption 2 (Unbiased gradient with bounded variance). *The stochastic gradient at each client is an unbiased estimate of the client's true gradient, i.e., $\mathbb{E}_{\zeta \sim \mathcal{D}_u^t}[g_u(\mathbf{w})] = \nabla f_u(\mathbf{w})$, where $\mathbb{E}[\cdot]$ is the expectation operator. Besides, the stochastic gradient has a bounded variance, i.e., $\mathbb{E}_{\zeta \sim \mathcal{D}_u^t}[\|g_u(\mathbf{w}) - \nabla f_u(\mathbf{w})\|^2] \leq \sigma^2$, for some $\sigma \geq 0$ and for all $u \in \mathcal{U}$.*

Assumption 3 (Bounded gradient divergence). *The divergence between the local and global gradients is bounded, i.e., $\|\nabla f_u(\mathbf{w}) - \nabla f(\mathbf{w})\|^2 \leq \varepsilon^2$, for some $\varepsilon \geq 0$ and $u \in \mathcal{U}$.*

While assumptions 1 and 2 are standard and widely used for the theoretical analysis of SGD [8], assumption 3 is widely used for the convergence analysis of FL [13], [33].

B. Convergence Analysis

We consider the expected average global gradient norm as an indicator of convergence of the proposed OSAFL algorithm.

Theorem 1. *Suppose the above assumptions hold. When the learning rates satisfy $\eta\tilde{\eta} \leq \frac{1}{\beta}$ and $\eta < \frac{1}{\sqrt{6}\beta\kappa}$, we have*

$$\frac{1}{T} \sum_{t=0}^{T-1} \mathbb{E}[\|\nabla f(\mathbf{w}^t)\|^2] \leq \frac{1}{T} \sum_{t=0}^{T-1} \left\{ \frac{1}{A^t} \left[\frac{2F^t}{\eta\tilde{\eta}} + \beta\eta\tilde{\eta}\sigma^2 \sum_{u=0}^{U-1} \alpha_u^2 (\Delta_u^t)^2 + 4\beta^2\eta^2\sigma^2 \sum_{u=0}^{U-1} \alpha_u \kappa_u^t B_u^t + 12\beta^2\eta^2\varepsilon^2 \sum_{u=0}^{U-1} \alpha_u B_u^t (\kappa_u^t)^2 \right] \right\}, \quad (13)$$

where $F^t = \mathbb{E}[f(\mathbf{w}^t)] - \mathbb{E}[f(\mathbf{w}^{t+1})]$, $A^t = 1 - 12\beta^2\eta^2\kappa^2 \sum_{u=0}^{U-1} \alpha_u B_u^t$ and $B_u^t = (\Delta_u^t)^2 - 2\Delta_u^t \lambda_u^t + 2(\lambda_u^t)^2$. Moreover $\mathbb{E}[\cdot]$ is the expectation operator that depends on the stochastic gradients³.

Sketch of Proof. Using the aggregation rule, we start with the β -Lipschitz smoothness assumption and write the following:

$$\mathbb{E}[f(\mathbf{w}^{t+1})] = \mathbb{E}[f(\mathbf{w}^t)] - \underbrace{\eta\tilde{\eta} \mathbb{E}\left[\left\langle \nabla f(\mathbf{w}^t), \sum_{u=0}^{U-1} \alpha_u \tilde{\mathbf{d}}_u^t \right\rangle\right]}_{T_1} +$$

³It is worth noting that the number of local SGD steps, i.e., κ_u^t , is assumed to be known in each global round. In practice, κ_u^t can also be stochastic depending on the varying wireless network parameters, such as the channel and available radio resources, to name a few.

$$\underbrace{\frac{\beta\eta^2\tilde{\eta}^2}{2} \mathbb{E}\left[\left\| \sum_{u=0}^{U-1} \alpha_u \tilde{\mathbf{d}}_u^t \right\|^2\right]}_{T_2}. \quad (14)$$

Then we simplify the T_1 and T_2 terms and get to

$$\begin{aligned} \mathbb{E}[f(\mathbf{w}^{t+1})] &\leq \mathbb{E}[f(\mathbf{w}^t)] - \frac{\eta\tilde{\eta}}{2} \mathbb{E}\left[\|\nabla f(\mathbf{w}^t)\|^2\right] + \\ &\quad \underbrace{\frac{\beta\eta^2\tilde{\eta}^2\sigma^2}{2} \sum_{u=0}^{U-1} \alpha_u^2 (\Delta_u^t)^2 + \frac{\eta\tilde{\eta}}{2} \mathbb{E}\left[\|\nabla f(\mathbf{w}^t) - \sum_{u=0}^{U-1} \alpha_u \tilde{\mathbf{h}}_u^t\|^2\right]}_{T_3} \\ &\quad - \frac{\eta\tilde{\eta}}{2} (1 - \beta\eta\tilde{\eta}) \mathbb{E}\left[\sum_{u=0}^{U-1} \alpha_u \tilde{\mathbf{h}}_u^t\right]^2, \end{aligned} \quad (15)$$

where $\tilde{\mathbf{h}}_u^t := \Delta_u^t \mathbf{h}_u^t = \Delta_u^t \frac{1}{\kappa_u^t} \sum_{\tau=0}^{\kappa_u^t-1} \nabla f_u(\mathbf{w}_u^{t,\tau})$. Then using $\eta\tilde{\eta} \leq \frac{1}{\beta}$, we have $(1 - \beta\eta\tilde{\eta}) \geq 0$, which allow us to drop the last term of (15). To that end, we simplify the T_3 term and get to the following

$$\begin{aligned} \frac{-2F^t}{\eta\tilde{\eta}} &\leq -\mathbb{E}\left[\|\nabla f(\mathbf{w}^t)\|^2\right] + \beta\eta\tilde{\eta}\sigma^2 \sum_{u=0}^{U-1} \alpha_u^2 (\Delta_u^t)^2 \\ &\quad + 2\beta^2 \sum_{u=0}^{U-1} \alpha_u \frac{B_u^t}{\kappa_u^t} \underbrace{\sum_{\tau=0}^{\kappa_u^t-1} \mathbb{E}\left[\|\mathbf{w}^t - \mathbf{w}_u^{t,\tau}\|^2\right]}_{T_4}. \end{aligned} \quad (16)$$

We then simplify the T_4 term and get to following
Simplify the T_4 term

$$\begin{aligned} \mathbb{E}\left[\|\nabla f(\mathbf{w}^t)\|^2\right] &\leq \frac{1}{A^t} \left[\frac{2F^t}{\eta\tilde{\eta}} + \beta\eta\tilde{\eta}\sigma^2 \sum_{u=0}^{U-1} \alpha_u^2 (\Delta_u^t)^2 + \right. \\ &\quad \left. 4\beta^2\eta^2\sigma^2 \sum_{u=0}^{U-1} \alpha_u \kappa_u^t B_u^t + 12\beta^2\eta^2\varepsilon^2 \sum_{u=0}^{U-1} \alpha_u B_u^t (\kappa_u^t)^2 \right]. \end{aligned} \quad (17)$$

From this, we get to (13) after averaging over time. Due to page limitations, the detailed proof is left in the supplementary materials. ■

Remark 2. *The terms inside the $[\cdot]$ in (13) have the following interpretations. The first diminishing term captures the changes in global loss functions between two consecutive rounds. The second and the third terms appear due to the bounded variance assumption of the stochastic gradients. Besides, the last term appears from the divergence between the local and global loss functions as a result of the statistical data heterogeneity.*

It is worth noting that the positive score in the second term of (13) appears from our aggregation rule. More specifically, since a client's normalized gradient gets scaled by its score Δ_u^t , which is non-negative, the multiplication of α_u and Δ_u^t is essentially the combined aggregation weight for a client. Moreover, since σ^2 appears from the bounded variance of the stochastic gradients and is multiplied by the learning rates, this term is expected to be significantly small⁴.

Corollary 1. *In addition to the conditions in Theorem 1, if the local learning rate satisfies $\eta < \frac{1}{2\beta\kappa\sqrt{3\sum_{u=0}^{U-1} \alpha_u B_u^t}}$, the average*

⁴If gradient descent is utilized to compute the true gradient over the client's entire dataset, which can be extremely time/resource consuming, σ^2 becomes zero, which means the second and third terms in (13) become 0.

global gradient norm is upper-bounded by

$$\frac{1}{T} \sum_{t=0}^{T-1} \mathbb{E} \left[\|\nabla f(\mathbf{w}^t)\|^2 \right] \leq \frac{1}{T} \sum_{t=0}^{T-1} \left[\frac{2F^t}{\eta \tilde{\eta}} + \beta \eta \tilde{\eta} \sigma^2 \sum_{u=0}^{U-1} \alpha_u^2 (\Delta_u^t)^2 + 4\beta^2 \eta^2 \sigma^2 \sum_{u=0}^{U-1} \alpha_u \kappa_u^t B_u^t + 12\beta^2 \eta^2 \varepsilon^2 \sum_{u=0}^{U-1} \alpha_u B_u^t (\kappa_u^t)^2 \right]. \quad (18)$$

Proof. When local learning rate η^t satisfy the above condition, we have $0 < (1 - 12\beta^2(\eta^t)^2 \kappa \sum_{u=0}^{U-1} \alpha_u B_u^t) < 1$. Using this fact in (17), we have

$$\mathbb{E} \left[\|\nabla f(\mathbf{w}^t)\|^2 \right] \leq \frac{2F^t}{\eta^t \tilde{\eta}^t} + \beta \eta^t \tilde{\eta}^t \sigma^2 \sum_{u=0}^{U-1} \alpha_u^2 (\Delta_u^t)^2 + 4\beta^2 (\eta^t)^2 \sigma^2 \sum_{u=0}^{U-1} \alpha_u \kappa_u^t B_u^t + 12\beta^2 (\eta^t)^2 \varepsilon^2 \sum_{u=0}^{U-1} \alpha_u B_u^t (\kappa_u^t)^2. \quad (19)$$

Then, averaging over time gives (18). \blacksquare

Remark 3. (Special Case) When the accumulated gradients are not scaled, i.e., $\Delta_u^t = 1$ for all t and $u \in \mathcal{U}$, Theorem 1 boils down to

$$\frac{1}{T} \sum_{t=0}^{T-1} \mathbb{E} \|\nabla f(\mathbf{w}^t)\|^2 \leq \frac{1}{T} \sum_{t=0}^{T-1} \left\{ \frac{1}{\tilde{A}^t} \left[\frac{2F^t}{\eta \tilde{\eta}} + \beta \eta \tilde{\eta} \sigma^2 \sum_{u=0}^{U-1} \alpha_u^2 + 4\beta^2 \eta^2 \sigma^2 \sum_{u=0}^{U-1} \alpha_u \kappa_u^t (1 - 2\lambda_u^t (1 - \lambda_u^t)) + 12\beta^2 \eta^2 \varepsilon^2 \sum_{u=0}^{U-1} \alpha_u (1 - 2\lambda_u^t (1 - \lambda_u^t)) (\kappa_u^t)^2 \right] \right\}, \quad (20)$$

where $\tilde{A}^t = 1 - 12\beta^2 \eta^2 \kappa^2 + 24\beta^2 \eta^2 \kappa^2 \sum_{u=0}^{U-1} \alpha_u \lambda_u^t (1 - \lambda_u^t)$. It is worth noting that OSAFL differs from FedAvg since the gradient similarity is explicitly calculated and utilized in our theoretical analysis in Theorem 1. However, if we assume $\lambda_u^t = 1$ for all clients⁵ and $\eta < \frac{1}{2\sqrt{3}\beta\kappa}$, (20) boils down to

$$\begin{aligned} \frac{1}{T} \sum_{t=0}^{T-1} \mathbb{E} \|\nabla f(\mathbf{w}^t)\|^2 &\leq \frac{1}{T} \sum_{t=0}^{T-1} \left\{ \left[\frac{2F^t}{\eta \tilde{\eta}} + \beta \eta \tilde{\eta} \sigma^2 \sum_{u=0}^{U-1} \alpha_u^2 + 4\beta^2 \eta^2 \sigma^2 \sum_{u=0}^{U-1} \alpha_u \kappa_u^t + 12\beta^2 \eta^2 \varepsilon^2 \sum_{u=0}^{U-1} \alpha_u (\kappa_u^t)^2 \right] \right\} \\ &= \frac{2(\mathbb{E}[f(\mathbf{w}^0)] - \mathbb{E}[f(\mathbf{w}^T)])}{\eta \tilde{\eta} T} + \beta \eta \tilde{\eta} \sigma^2 \sum_{u=0}^{U-1} \alpha_u^2 + \\ &\quad \sum_{t=0}^{T-1} \frac{1}{T} 4\beta^2 \eta^2 \left[\sigma^2 \sum_{u=0}^{U-1} \alpha_u \kappa_u^t + 3\varepsilon^2 \sum_{u=0}^{U-1} \alpha_u (\kappa_u^t)^2 \right], \quad (21) \end{aligned}$$

which is the equivalent convergence bound of general FedAvg algorithm under full client participation with two sided learning rate [34].

The above analysis suggests that the convergence rate is intricately related to the exponent of the gradient similarity λ_u^t , score Δ_u^t and other hyper-parameters. As such, it is essential to optimize the score Δ_u^t of the clients in order to improve the convergence rate of the proposed OSAFL algorithm.

⁵In theory, this is only possible if \mathbf{d}_u^t and \mathbf{d}^t are orthogonal. However, we stress that our proposed algorithm is different than FedAvg, and this measure only shows how OSAFL can be reduced to FedAvg.

C. Online Score Optimization

In order to facilitate the learning process, we want to minimize the right-hand side of (13). As such, we pose the following optimization problem:

$$\begin{aligned} \text{minimize} \quad & \theta := \frac{1}{T} \sum_{t=0}^{T-1} \left\{ \frac{1}{A^t} \left[\frac{2F^t}{\eta \tilde{\eta}} + \beta \eta \tilde{\eta} \sigma^2 \sum_{u=0}^{U-1} \alpha_u^2 (\Delta_u^t)^2 + 4\beta^2 \eta^2 \sigma^2 \sum_{u=0}^{U-1} \alpha_u \kappa_u^t B_u^t + 12\beta^2 \eta^2 \varepsilon^2 \sum_{u=0}^{U-1} \alpha_u B_u^t (\kappa_u^t)^2 \right] \right\} \quad (22) \\ \text{subject to} \quad & \Delta_u^t > 0, \quad \forall u, t, \quad (22a) \end{aligned}$$

where θ is essentially the right-hand side of (13), and the constraint is enforced to ensure positive weighting of the normalized gradient updates of the clients.

Alas, this original optimization problem has a fractional objective function and is non-convex, which makes it hard to solve optimally. Therefore, instead of solving this fractional objective function, following standard practice [14], we convert the objective function as follows:

$$\begin{aligned} \tilde{\theta} := \frac{1}{T} \sum_{t=0}^{T-1} \left\{ \left[\frac{2F^t}{\eta \tilde{\eta}} + \beta \eta \tilde{\eta} \sigma^2 \sum_{u=0}^{U-1} \alpha_u^2 (\Delta_u^t)^2 + 4\beta^2 \eta^2 \sigma^2 \sum_{u=0}^{U-1} (\alpha_u \kappa_u^t B_u^t + 12\beta^2 \eta^2 \varepsilon^2 \sum_{u=0}^{U-1} \alpha_u B_u^t (\kappa_u^t)^2) - \psi A^t \right] \right\}, \quad (23) \end{aligned}$$

where ψ is some positive hyper-parameter. Thus, we want to optimize the following problem approximately.

$$\begin{aligned} \text{minimize} \quad & \tilde{\theta} \quad (24) \\ \text{subject to} \quad & \Delta_u^t \geq 0, \quad \forall u, t. \quad (24a) \end{aligned}$$

However, recall that $A^t = 1 - 12\beta^2 \eta^2 \kappa^2 \sum_{u=0}^{U-1} \alpha_u B_u^t$ and $B_u^t = (\Delta_u^t)^2 - 2\Delta_u^t \lambda_u^t + 2(\lambda_u^t)^2$. This objective function is, therefore, dependent on the exponent of the gradient similarities and the scores of the clients for all T FL rounds. Naturally, we cannot know the future gradients due to the randomness in local SGD steps κ_u^t , dynamic training dataset \mathcal{D}_u^t and data sampling for the stochastic gradient calculations. Moreover, the old training samples that get deleted due to limited storage are lost forever. Therefore, (24) still cannot be solved optimally before the training begins. As such, we seek an approximate solution strategy that allows us to approximately solve the following objective function in every FL round t .

$$\begin{aligned} \hat{\theta} := \beta \eta \tilde{\eta} \sigma^2 \sum_{u=0}^{U-1} \alpha_u^2 (\Delta_u^t)^2 + 4\beta^2 \eta^2 \sigma^2 \sum_{u=0}^{U-1} \alpha_u \kappa_u^t B_u^t + 12\beta^2 \eta^2 \varepsilon^2 \sum_{u=0}^{U-1} \alpha_u B_u^t (\kappa_u^t)^2 - \psi A^t. \quad (25) \end{aligned}$$

Therefore, the reformulated problem is written as

$$\begin{aligned} \text{minimize} \quad & \hat{\theta} \quad (26) \\ \text{subject to} \quad & \Delta_u^t \geq 0, \quad \forall u. \quad (26a) \end{aligned}$$

To that end, we focus on the solution of problem (26). Let us define the dual function as

$$\begin{aligned} L(\Delta^t) := & \beta \eta \tilde{\eta} \sigma^2 \sum_{u=0}^{U-1} \alpha_u^2 (\Delta_u^t)^2 + 4\beta^2 \eta^2 \sigma^2 \sum_{u=0}^{U-1} \alpha_u \kappa_u^t B_u^t + 12\beta^2 \eta^2 \varepsilon^2 \sum_{u=0}^{U-1} \alpha_u B_u^t (\kappa_u^t)^2 - \psi A^t - \sum_{u=0}^{U-1} \gamma_u^t \Delta_u^t, \quad (27) \end{aligned}$$

Algorithm 2: Get-Online-Score

Input: Global round index t , score update interval Υ , normalized accumulated gradients $\{\mathbf{d}_u^t\}_{u=0}^{U-1}$ and \mathbf{d}^t

```

1 Initiate  $\boldsymbol{\lambda}^0 = \{\lambda_u^0\}_{u=0}^{U-1} = \mathbf{0} \in \mathbb{R}^U$ 
2 if  $t = 0$  // Initialize the score
3 then
4   for  $u = 0$  to  $U - 1$  do
5     Calculate  $\tilde{\lambda}_u^t$  using (11)
6      $\lambda_u^t \leftarrow \exp(\tilde{\lambda}_u^t)$ 
7      $\Delta_u^t \leftarrow \lambda_u^t$ 
8   end
9 else
10  if  $(t+1) \bmod \Upsilon = 0$  // Score update round
11  then
12    for  $u = 0$  to  $U - 1$  do
13      Calculate  $\tilde{\lambda}_u^t$  using (11)
14       $\lambda_u^t = \lambda_u^{t-1} + \exp(\tilde{\lambda}_u^t)$  // Add new weight
15       $\Delta_u^t \leftarrow \lambda_u^t / \Upsilon$  // Update the score
16    end
17    Reset  $\boldsymbol{\lambda}^t = \{\lambda_u^t\}_{u=0}^{U-1} = \mathbf{0} \in \mathbb{R}^U$ 
18  else
19    for  $u = 0$  to  $U - 1$  do
20      Repeat steps 13 and 14
21       $\Delta_u^t \leftarrow \Delta_u^{t-1}$  // No change in scores
22    end
23  end
24 end

```

Output: Scores $\{\Delta_u^t\}_{u=0}^{U-1}$

where $\gamma_u^t \geq 0$ is a Lagrange multiplier [35, Chapter 5]. Then, from the stationarity condition [35, Chapter 5] of the Karush–Kuhn–Tucker (KKT) conditions, we write the following.

$$\frac{\partial L(\Delta_u^t)}{\partial \Delta_u^t} = 2\beta\Delta_u^t\eta\tilde{\eta}\sigma^2\alpha_u^2 + 8\beta^2\eta^2(\sigma^2 + 3\kappa\varepsilon^2)\alpha_u\kappa_u^t(\Delta_u^t - \lambda_u^t) + 24\psi\beta^2\eta^2\kappa^2\alpha_u(\Delta_u^t - \lambda_u^t) - \gamma_u^t = 0. \quad (28)$$

After solving (28), we have

$$\Delta_u^t = \frac{\gamma_u^t + C_1\lambda_u^t}{2\beta\eta\tilde{\eta}\sigma^2\alpha_u^2 + C_1}, \quad (29)$$

where $C_1 = 8\beta^2\eta^2(\sigma^2 + 3\kappa\varepsilon^2)\alpha_u\kappa_u^t + 24\psi\beta^2\eta^2\kappa^2\alpha_u$.

Note that (29) contains many hyper-parameters that come from the three standard assumptions we made to derive the convergence rate. Therefore, the exact value for the optimal Δ_u^t cannot be determined. However, we observe the following from (29).

$$\begin{aligned} \Delta_u^t &= \frac{\gamma_u^t}{2\beta\eta\tilde{\eta}\sigma^2\alpha_u^2 + C_1} + \frac{C_1\lambda_u^t}{2\beta\eta\tilde{\eta}\sigma^2\alpha_u^2 + C_1} \\ &\propto \text{Constant} + \left[\frac{C_1}{2\beta\eta\tilde{\eta}\sigma^2\alpha_u^2 + C_1} \right] \lambda_u^t \\ &\propto \lambda_u^t. \end{aligned} \quad (30)$$

This essentially means that Δ_u^t is proportional to some constant plus the exponent of the gradient similarity, i.e., λ_u^t . As such, we can also say that the optimal *score* of a client shall be proportional to λ_u^t .

It is worth noting that updating the score in every global round may not be suitable under system and data heterogeneity. In particular, two primary factors that influence the local gradients are (a) the evolution of the dynamic dataset \mathcal{D}_u^t and (b) the number of SGD steps κ_u^t . Therefore, the local

gradients may cause rapid fluctuations in the client's score due to the randomness of these two key factors. Intuitively, this fluctuation shall depend on the degree of randomness. As such, we use Algorithm 2, which allows us to control how frequently this score is updated. The algorithm is general and can be modified based on the underlying characteristics of dataset evolution and the choice of the number of local SGD steps.

Notice that we start with assigning a vector of zeros $\boldsymbol{\lambda}^0 = \{\lambda_u^0\}_{u=0}^{U-1} \in \mathbb{R}^U$ to store the values of the λ_u^t . At the first global FL round, we calculate the gradient similarity and reassign the value of λ_u^t . Moreover, the *score* Δ_u^t is set to be λ_u^t . This *score* is next updated every Υ global FL rounds. More specifically, for every FL round that is not a *score* update round, we keep accumulating the client's λ_u^t and return the previously calculated *score*, i.e., $\Delta_u^t \leftarrow \Delta_u^{t-1}$. When we reach a *score* update round, we simply take the average of the accumulated λ_u^t as the *score* Δ_u^t of the client and reset the $\boldsymbol{\lambda}^t$ vector to zeros.

Remark 4. Algorithm 2 does not need to stack the gradient similarities for all Υ rounds since line 14 only adds the λ_u^t and has a time complexity of $\mathcal{O}(1)$. Therefore, once the CS initiates the $\boldsymbol{\lambda}^0$, which has a space complexity of $\mathcal{O}(N)$, the new values can be added to the corresponding index and does not incur any additional space complexity.

IV. SIMULATION RESULTS AND DISCUSSIONS

We use different ML models on two different tasks. Particularly, since our OSAFL algorithm is tailored for wireless applications, and there is no real-world dataset for such applications; we consider content request prediction in wireless video caching networks [3] as our first task⁶. Besides, we also consider a general image classification task to show the effectiveness of the proposed OSAFL algorithm for a more general application. We use six state-of-the-art baselines, namely, (1) FedAvg [1], (2) FedProx [11], (3) FedNova [12], (4) AFA [13], (5) FedDisco [14] and (6) SCAFFOLD [10], on six different datasets for the above two tasks. It is worth noting that these algorithms were mainly designed for static datasets. However, we will use these widely used baselines in this work since, to our best knowledge, no prior works⁷ considered the system models and time-varying datasets that we have considered in this paper. Finally, we also compare the performance with centralized ML, more specifically, with centralized SGD, assuming that the training samples available at the clients in each global round are centrally available to a *Genie*.

A. Performance Evaluation in Video Caching Task

The task is to predict the users' to-be-requested content ID based on the historical content request information.

⁶However, our proposed algorithm can easily be applied to other time-varying datasets for other wireless/different applications.

⁷We note that our previous work [3] considered time-varying datasets and considered a hierarchical FL algorithm where aggregations at different tiers were modeled following FedAvg, which is a generalization of optimization problem (3).

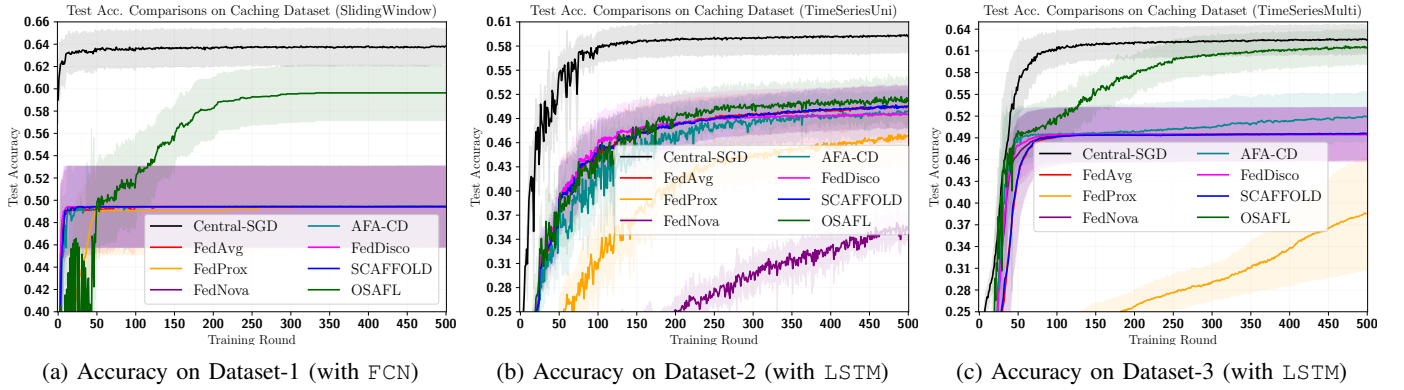


Fig. 2: Test accuracy comparisons on video caching datasets (from 5 independent trials)

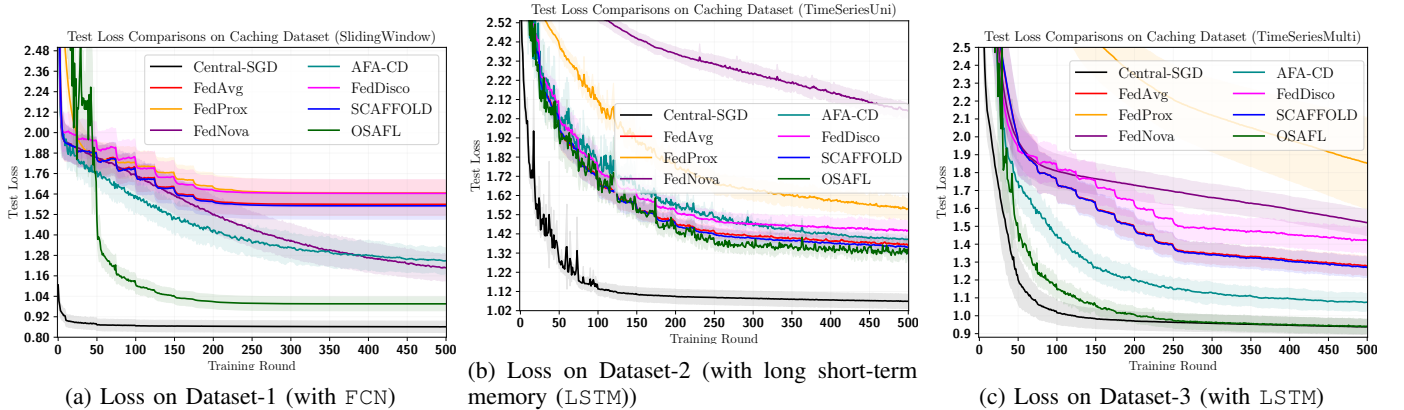


Fig. 3: Test loss comparisons on video caching datasets (from 5 independent trials)

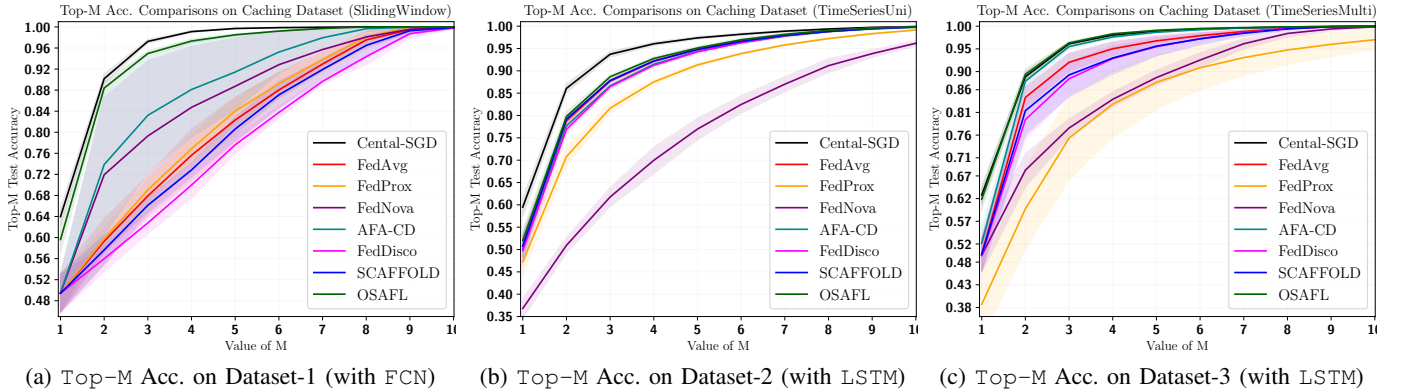


Fig. 4: Top-M test accuracy comparisons on video caching datasets (from 5 independent trials)

1) *Simulation Setting:* We consider $U = 100$ clients and $T = 500$ global rounds for this task. Each client's maximum training sample storage capacity, i.e., D_u , is uniformly randomly drawn from $[500, 1500]$. Besides, $p_{u,ac} \in [0.3, 0.8]$ for all clients and $E_u = E = 5$. In between two global rounds, the clients receive new training samples following [3] and remove the oldest stored sample, i.e., based on a FIFO policy⁸. For local model training, the clients use a batch size of 32

⁸Other policy can also be easily incorporated. However, since it is a prediction task, we assume removing the sample following the FIFO policy to maintain the sequential request order in the dataset.

and 10 mini-batches. Besides, the number of SGD steps, i.e., κ_u^t , for each client is uniformly randomly drawn from $[1, 15]$ in every global round. Note that these parameters are chosen to mimic the practical resource constraints in wireless networks. The following three synthetic datasets, which follow the same content request generation process but differ in terms of the feature and label information, were considered due to the unavailability of real-world datasets with spatio-temporal information [3].

Dataset-1: This dataset is generated based on the method described in [3]. In particular, this dataset has a total of

TABLE I: Test Performance Comparisons on Synthetic Video Caching Datasets (Average of 5 Independent Trials)

| Type | Algorithms | Dataset-1 (with FCN) | | Dataset-2 (with LSTM) | | Dataset-3 (with LSTM) | |
|-----------|----------------------|---------------------------------------|---------------------------------------|---------------------------------------|---------------------------------------|---------------------------------------|---------------------------------------|
| | | Test Acc. \uparrow | Test Loss \downarrow | Test Acc. \uparrow | Test Loss \downarrow | Test Acc. \uparrow | Test Loss \downarrow |
| Central | SGD | 0.6397 \pm 0.0161 | 0.8617 \pm 0.0327 | 0.5950 \pm 0.0213 | 1.0709 \pm 0.0378 | 0.6279 \pm 0.0196 | 0.9404 \pm 0.0437 |
| Federated | OSA-FL (Ours) | 0.5963 \pm 0.0247 | 0.9963 \pm 0.0402 | 0.5201 \pm 0.0249 | 1.3094 \pm 0.0264 | 0.6185 \pm 0.0231 | 0.9391 \pm 0.0396 |
| | FedAvg [1] | 0.4942 \pm 0.0362 | 1.9215 \pm 0.0971 | 0.5078 \pm 0.0256 | 1.3623 \pm 0.0283 | 0.4973 \pm 0.0359 | 1.3443 \pm 0.0737 |
| | AFA-CD [13] | 0.4951 \pm 0.0363 | 1.5663 \pm 0.3004 | 0.5012 \pm 0.0265 | 1.3963 \pm 0.0220 | 0.5217 \pm 0.0330 | 1.0740 \pm 0.0494 |
| | FedNova [12] | 0.4947 \pm 0.0363 | 1.5891 \pm 0.3763 | 0.3681 \pm 0.0221 | 2.0760 \pm 0.0488 | 0.4949 \pm 0.0370 | 1.7491 \pm 0.0657 |
| | FedProx [11] | 0.4937 \pm 0.0367 | 1.7990 \pm 0.0951 | 0.4728 \pm 0.0315 | 1.5534 \pm 0.0570 | 0.3869 \pm 0.0781 | 1.8560 \pm 0.2567 |
| | FedDisco [14] | 0.4942 \pm 0.0362 | 2.0156 \pm 0.0924 | 0.4976 \pm 0.0335 | 1.4439 \pm 0.0569 | 0.4950 \pm 0.0371 | 1.5677 \pm 0.0849 |
| | SCAFFOLD [10] | 0.4942 \pm 0.0362 | 1.9606 \pm 0.0631 | 0.5076 \pm 0.0257 | 1.3531 \pm 0.0341 | 0.4970 \pm 0.0367 | 1.4180 \pm 0.1703 |

256 video files from 8 different genres. Each training sample has a feature set consisting of 43 elements spanning from some information about the user’s content request and the requested content⁹ and a one-hot-encoded label to indicate the requested content ID. Similar to [3], we consider a sliding window technique to predict the next video request of the clients. Besides, similar to [3], we use a fully connected neural network (FCN) with rectified linear (ReLU) activation function as the ML model for this dataset. We use SGD optimizer with an initial local learning rate $\eta = 0.5$. Besides, we use an initial $\tilde{\eta} = 10$ for the global SGD step at the CS. The local and global learning rates are reduced by 50% and 5%, respectively, in every 25 global round. Moreover, we find that OSAFL gives the best result with the above hyper-parameters when $Y = 3$.

Dataset-2: This dataset essentially contains only the user’s requested content IDs. We basically use the same content request generation patterns as in dataset 1, except that we now pose the content request prediction as a uni-variate time-series prediction. Therefore, we use a LSTM model with 2 recurrent layers with a hidden state size of 1024, followed by a fully connected (FC) layer with an output size equal to the number of video files, i.e., 256. Similar to the above case, we use SGD optimizer with $\eta = 0.1$ for the local model training and $\tilde{\eta} = 6$ for the global SGD step. Besides, the η and $\tilde{\eta}$ are reduced by 25% and 5% in every 25 global rounds till the 250th global round. Moreover, we use $Y = 5$ for this dataset and model.

Dataset-3: For this dataset, we essentially combine the feature set and the corresponding label to predict the future video request IDs of the users using multi-variate time-series analysis. As such, we also use the same LSTM model architecture except that the input size is equivalent to the number of features per sample as our ML model for this dataset. For the local model training, we use the same setting as in the second dataset. Besides, we use $\tilde{\eta} = 8$ and reduce it by 2% in every 25 global rounds till the 250th global round. Moreover, we use $Y = 3$.

2) *Performance Comparisons:* The performance of the algorithms can vary across different datasets and ML models. In our proposed OSAFL algorithm, since each client’s *score* is calculated based on the gradient similarities as shown in (30), the initial few updates in the global ML model following (8) may lead to some initial fluctuations. Besides, the dynamic dataset causes changes in the training samples, and different local SGD rounds of the clients may further contribute to different local gradients in different clients. Therefore, these

factors may play their roles in such initial fluctuations.

Our simulation results in Fig. 2 and Fig. 3 also suggest the above trends. In particular, we experience higher fluctuations with the FCN model on dataset 1 of the video caching task, while much lower fluctuations with the LSTM models on datasets 2 and 3. Intuitively, the sliding-window technique with FCN may require additional training rounds to understand the intricate time properties, which can also contribute to the initial fluctuations. On the other hand, LSTM is specifically designed for time series analysis, allowing it to learn the intricate temporal relations in the video content requests. We also observe this in the results from these models on the three datasets. For example, the FCN model fluctuates rapidly until around the 50th global round, while the LSTM model provided stable performance in both dataset 2 and dataset 3 almost from the beginning. Note that all of the 7 FL algorithms have performance deviations from the centralized SGD performance in Fig. 2 and Fig. 3, which is indeed expected since training samples are not available centrally due to privacy issues. However, our proposed OSAFL has the closest performance to that of the centralized SGD compared to the 6 FL baselines in terms of test accuracy and test loss in all three datasets.

To that end, we use the global model that gives the best test accuracy to evaluate more test performances. First, we use this trained global model to find the Top-M accuracy, which is essentially the probability that the true requested content is within the Top-M predicted content. Therefore, a high M value shall lead to high test accuracy. From both the FCN and LSTM models’ performances on the three considered datasets in Fig. 4, we observe that our proposed solution has the closest performance to that of the central SGD performance for all considered values of M . For example, the Top-4 accuracy with the centralized SGD, OSAFL, FedAvg, AFA, FedNova, FedProx, FedDisco and SCAFFOLD are 99.11%, 97.33%, 75.64%, 88.12%, 84.73%, 76.88%, 69.98% and 72.84%, respectively, on dataset 1. Besides, on dataset 2, the Top-4 test accuracies are 96.05%, 92.76%, 92.14%, 91.46%, 69.97%, 87.52%, 91.23% and 92.19%, respectively, while they are 98.05%, 98.33%, 95.03%, 97.63%, 83.88%, 82.83%, 92.86% and 92.99%, respectively, on dataset 3.

Moreover, we have reported the best test accuracy and the corresponding test loss from all 7 baselines in Table I. For convenience, the best and second best performances are highlighted in green and red, respectively. Note that our proposed OSAFL algorithm delivers about 10.12%, 1.23% and 9.68% higher test accuracy than the second best accuracy from the 6 baselines in the 3 datasets, respectively; about

⁹The complete feature set is listed in [3, Section V-A].

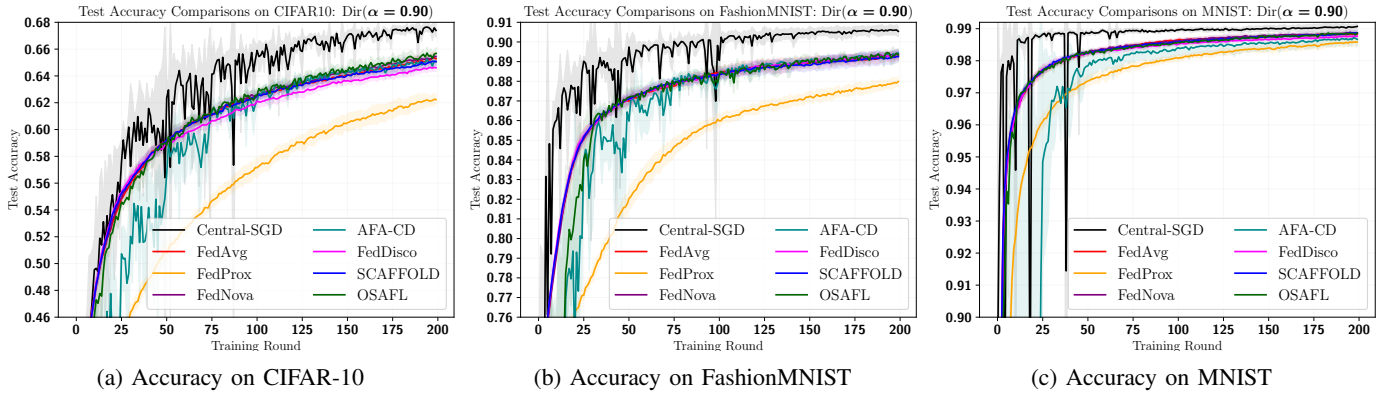


Fig. 5: Test accuracy comparisons on image classification tasks (from 5 independent trials with FIFO policy)

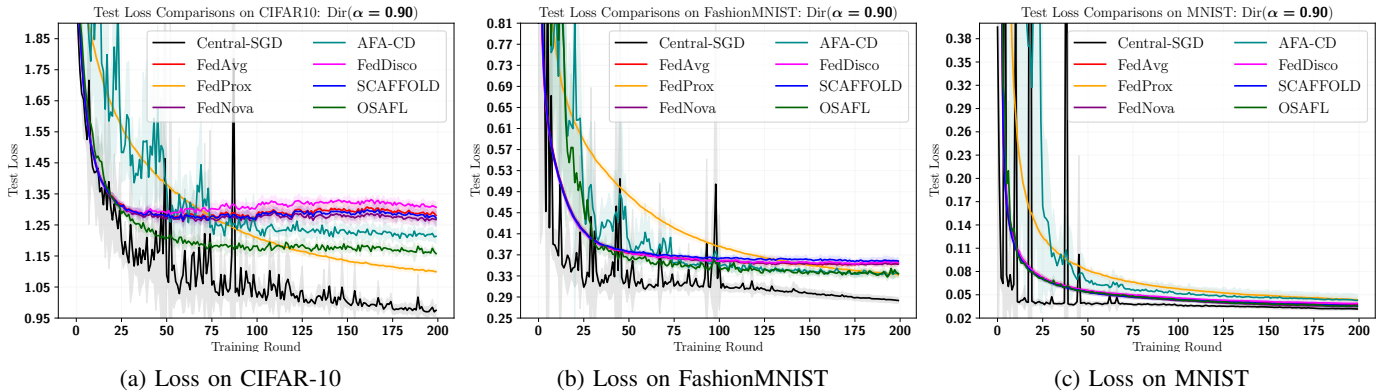


Fig. 6: Test loss comparisons on image classification tasks (from 5 independent trials with FIFO policy)

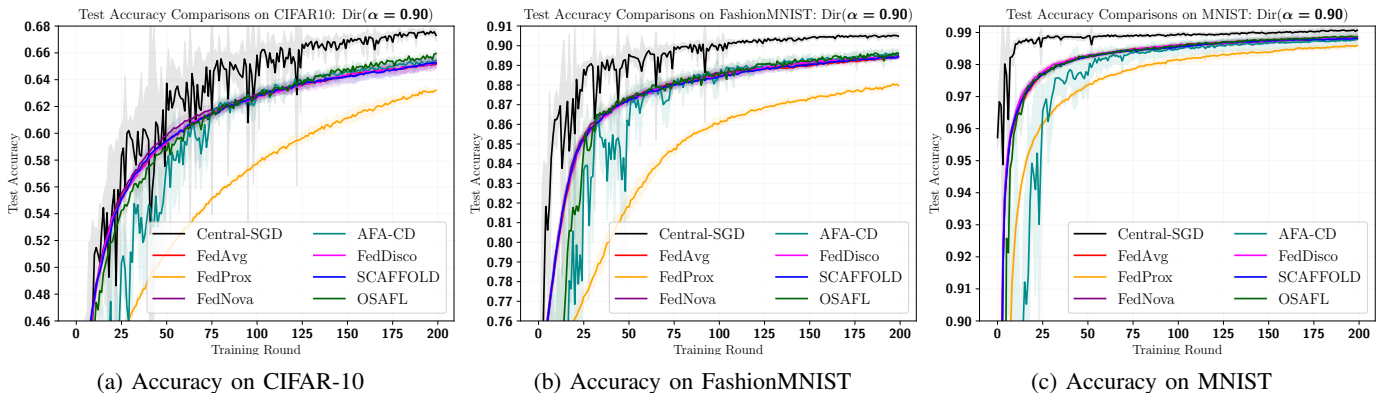


Fig. 7: Test accuracy comparisons on image classification tasks (from 5 independent trials with TrimTopLabel policy)

36.39% 3.23% and 12.56% lower test loss, respectively in the 3 datasets.

B. Performance Evaluation in Image Classification Task

We now consider image classification task using 3 popular datasets: (1) CIFAR-10 [9], (2) Fashion-MNIST (FMNIST) [36] and (3) MNIST [37]. It is worth noting that wireless applications can differ significantly from image classification tasks. However, we consider the image classification task with these widely popular datasets to evaluate the performances of our proposed algorithm in a more general application.

1) *Simulation Parameters:* We consider 50 clients¹⁰ and distribute the training samples using a symmetric Dirichlet distribution $\text{Dir}(\alpha)$ with concentration parameter α and following the strategy as in [18]. Note that we distribute the entire training dataset across the clients in a non-overlapping manner before starting the training and assume training samples arrive

¹⁰Given that there are a fixed number of training samples in these datasets, which are distributed among the clients so that each client has non-overlapping samples, and some new training samples need to arrive in every global FL round, 50 is an appropriate number of clients for these datasets. It is possible to increase the number of clients, but that may force the reduction of the client's dataset size D_u to inherit the properties of our system model.

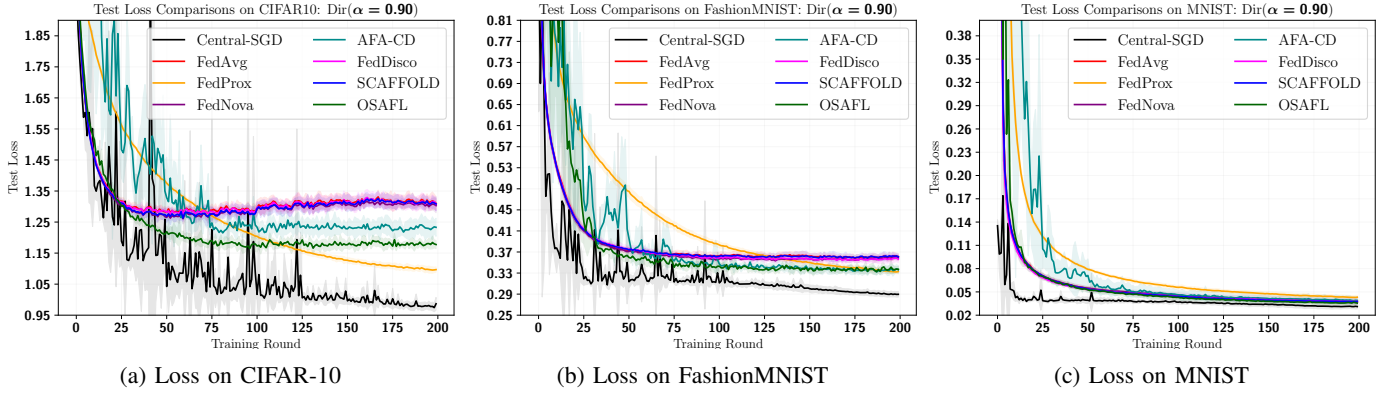


Fig. 8: Test loss comparisons on image classification tasks (from 5 independent trials with TrimTopLabel policy)

TABLE II: Test Performance Comparisons: FIFO (Average of 5 Independent Trials)

| Dataset | Type | Algorithms | Test Accuracy \uparrow | | | Test Loss \downarrow | | |
|---------------|-----------|---------------------|---------------------------------------|---------------------------------------|---------------------------------------|---------------------------------------|---------------------------------------|---------------------------------------|
| | | | Dir($\alpha = 0.5$) | Dir($\alpha = 0.9$) | Dir($\alpha = 10$) | Dir($\alpha = 0.5$) | Dir($\alpha = 0.9$) | Dir($\alpha = 10$) |
| CIFAR-10 | Central | SGD | 0.6796 \pm 0.0042 | 0.6785 \pm 0.0025 | 0.6789 \pm 0.0026 | 0.9711 \pm 0.0141 | 0.9686 \pm 0.0153 | 0.9644 \pm 0.0082 |
| | Federated | OSAFL (Ours) | 0.6529 \pm 0.0032 | 0.6591 \pm 0.0035 | 0.6679 \pm 0.0030 | 1.1665 \pm 0.0148 | 1.1632 \pm 0.0040 | 1.1408 \pm 0.0184 |
| | | FedAvg [1] | 0.6401 \pm 0.0049 | 0.6539 \pm 0.0040 | 0.6607 \pm 0.0044 | 1.3093 \pm 0.0158 | 1.2916 \pm 0.0271 | 1.2856 \pm 0.0131 |
| | | AFA-CD [13] | 0.6465 \pm 0.0029 | 0.6538 \pm 0.0027 | 0.6577 \pm 0.0048 | 1.2145 \pm 0.0139 | 1.2134 \pm 0.0242 | 1.2189 \pm 0.0290 |
| | | FedNova [12] | 0.6458 \pm 0.0037 | 0.6546 \pm 0.0021 | 0.6586 \pm 0.0027 | 1.2795 \pm 0.0186 | 1.2696 \pm 0.0243 | 1.2916 \pm 0.0040 |
| | | FedProx [11] | 0.6143 \pm 0.0035 | 0.6235 \pm 0.0044 | 0.6430 \pm 0.0027 | 1.1296 \pm 0.0117 | 1.1004 \pm 0.0068 | 1.0712 \pm 0.0109 |
| | | FedDisco [14] | 0.6363 \pm 0.0035 | 0.6472 \pm 0.0028 | 0.6577 \pm 0.0044 | 1.3395 \pm 0.0213 | 1.3030 \pm 0.0143 | 1.2974 \pm 0.0143 |
| | | SCAFFOLD [10] | 0.6414 \pm 0.0065 | 0.6517 \pm 0.0036 | 0.6598 \pm 0.0066 | 1.3047 \pm 0.0153 | 1.2822 \pm 0.0181 | 1.2790 \pm 0.0274 |
| Fashion-MNIST | Central | SGD | 0.9041 \pm 0.0011 | 0.9072 \pm 0.0021 | 0.9055 \pm 0.0018 | 0.2978 \pm 0.0109 | 0.2870 \pm 0.0070 | 0.2876 \pm 0.0048 |
| | Federated | OSAFL (Ours) | 0.8934 \pm 0.0010 | 0.8962 \pm 0.0012 | 0.8981 \pm 0.0014 | 0.3353 \pm 0.0091 | 0.3308 \pm 0.0042 | 0.3223 \pm 0.0080 |
| | | FedAvg [1] | 0.8908 \pm 0.0014 | 0.8936 \pm 0.0025 | 0.8971 \pm 0.0015 | 0.3618 \pm 0.0092 | 0.3542 \pm 0.0053 | 0.3560 \pm 0.0065 |
| | | AFA-CD [13] | 0.8938 \pm 0.0015 | 0.8951 \pm 0.0015 | 0.8992 \pm 0.0015 | 0.3376 \pm 0.0071 | 0.3339 \pm 0.0057 | 0.3286 \pm 0.0057 |
| | | FedNova [12] | 0.8908 \pm 0.0035 | 0.8943 \pm 0.0013 | 0.8966 \pm 0.0011 | 0.3569 \pm 0.0093 | 0.3529 \pm 0.0009 | 0.3565 \pm 0.0048 |
| | | FedProx [11] | 0.8750 \pm 0.0022 | 0.8800 \pm 0.0024 | 0.8833 \pm 0.0017 | 0.3465 \pm 0.0059 | 0.3330 \pm 0.0059 | 0.3283 \pm 0.0038 |
| | | FedDisco [14] | 0.8901 \pm 0.0027 | 0.8941 \pm 0.0021 | 0.8973 \pm 0.0009 | 0.3680 \pm 0.0121 | 0.3560 \pm 0.0031 | 0.3553 \pm 0.0099 |
| | | SCAFFOLD [10] | 0.8899 \pm 0.0027 | 0.8931 \pm 0.0032 | 0.8965 \pm 0.0013 | 0.3570 \pm 0.0087 | 0.3609 \pm 0.0080 | 0.3544 \pm 0.0040 |
| MNIST | Central | SGD | 0.9905 \pm 0.0008 | 0.9911 \pm 0.0008 | 0.9914 \pm 0.0003 | 0.0346 \pm 0.0030 | 0.0330 \pm 0.0040 | 0.0323 \pm 0.0021 |
| | Federated | OSAFL (Ours) | 0.9881 \pm 0.0003 | 0.9891 \pm 0.0005 | 0.9896 \pm 0.0002 | 0.0385 \pm 0.0010 | 0.0351 \pm 0.0014 | 0.0336 \pm 0.0007 |
| | | FedAvg [1] | 0.9877 \pm 0.0005 | 0.9886 \pm 0.0005 | 0.9893 \pm 0.0004 | 0.0386 \pm 0.0015 | 0.0370 \pm 0.0020 | 0.0365 \pm 0.0023 |
| | | AFA-CD [13] | 0.9857 \pm 0.0035 | 0.9874 \pm 0.0018 | 0.9896 \pm 0.0004 | 0.0481 \pm 0.0115 | 0.0436 \pm 0.0080 | 0.0357 \pm 0.0013 |
| | | FedNova [12] | 0.9880 \pm 0.0010 | 0.9890 \pm 0.0008 | 0.9892 \pm 0.0004 | 0.0392 \pm 0.0042 | 0.0350 \pm 0.0010 | 0.0354 \pm 0.0019 |
| | | FedProx [11] | 0.9850 \pm 0.0006 | 0.9861 \pm 0.0012 | 0.9874 \pm 0.0011 | 0.0458 \pm 0.0012 | 0.0440 \pm 0.0032 | 0.0405 \pm 0.0007 |
| | | FedDisco [14] | 0.9878 \pm 0.0008 | 0.9879 \pm 0.0007 | 0.9892 \pm 0.0005 | 0.0404 \pm 0.0030 | 0.0389 \pm 0.0022 | 0.0351 \pm 0.0019 |
| | | SCAFFOLD [10] | 0.9880 \pm 0.0004 | 0.9889 \pm 0.0007 | 0.9899 \pm 0.0007 | 0.0393 \pm 0.0015 | 0.0361 \pm 0.0027 | 0.0343 \pm 0.0020 |

from these assigned data for simplicity. Denote this dataset for client u by $\mathcal{D}_{u,\text{all}}$. We randomly sample each client's dataset size $D_u \in [256, 384]$. Each client has a new sample arrival probability, $p_{u,\text{ac}}$, drawn uniformly randomly from $[0.3, 0.8]$. As such, we determine E_u as

$$E_u := \min \left\{ \left\lfloor \frac{(|\mathcal{D}_{u,\text{all}}| - D_u)}{T} \right\rfloor, 5 \right\}, \quad (31)$$

where $\lfloor \cdot \rfloor$ denotes the floor operation. Besides, the training batch size is 32, 5 mini-batches are randomly selected during each local round and $\kappa_u^t \in [1, 15]$. We consider three concentration parameters, i.e., $\alpha = \{0.5, 0.9, 10\}$, for the Dirichlet distribution. Furthermore, the SGD optimizer with initial $\eta = 0.1$ is used, while the global learning rate $\tilde{\eta}$ is set to 5 for CIFAR-10 and MNIST datasets. For the FMNIST dataset, $\tilde{\eta} = 6$ when $\text{Dir}(\alpha = 0.5)$ or $\text{Dir}(\alpha = 0.9)$, and $\tilde{\eta} = 5$ when $\text{Dir}(\alpha = 10)$. Moreover, the local learning rates are decreased by 10%, 5% and 5% in every 20 global FL rounds for CIFAR-10, FMNIST and MNIST datasets, respectively, till 150th rounds. Each FL algorithm is trained for

$T = 200$ global rounds with a simple convolutional neural network (CNN) model that has the following architecture: Conv2d (#Channels, 128) \rightarrow ReLU() \rightarrow MaxPool2d() \rightarrow Conv2d(128, 64) \rightarrow ReLU() \rightarrow MaxPool2d \rightarrow FC (256, 256) \rightarrow ReLU \rightarrow FC (256, #Labels).

2) *Performance Comparisons:* We consider two data deletion policies: (1) FIFO policy and (2) TrimTopLabel policy for this image classification task. The FIFO policy is the same as in the video caching task, and recall that in TrimTopLabel, a client removes samples from its top labels in the current local dataset \mathcal{D}_u^t . Since image classification has no time dependency, it is also possible to consider other data deletion policies¹¹.

Due to statistical data heterogeneity, clients' training sam-

¹¹For example, the data sample may also be removed according to the label distributions within the current dataset \mathcal{D}_u^t . However, in some extreme cases, that policy may still remove some rare labels since the policy is probabilistic. Moreover, in our simulation, we noticed better results with the TrimTopLabel policy.

TABLE III: Test Performance Comparisons: TrimTopLabel (Average of 5 Independent Trials)

| Dataset | Type | Algorithms | Test Accuracy \uparrow | | | Test Loss \downarrow | | |
|---------------|-----------|---------------------|-------------------------------------|-------------------------------------|-------------------------------------|-------------------------------------|-------------------------------------|-------------------------------------|
| | | | Dir($\alpha = 0.5$) | Dir($\alpha = 0.9$) | Dir($\alpha = 10$) | Dir($\alpha = 0.5$) | Dir($\alpha = 0.9$) | Dir($\alpha = 10$) |
| CIFAR-10 | Central | SGD | 0.6776 \pm 0.0015 | 0.6778 \pm 0.0021 | 0.6784 \pm 0.0030 | 0.9747 \pm 0.0059 | 0.9781 \pm 0.0122 | 0.9726 \pm 0.0037 |
| | | OSAFL (Ours) | 0.6531\pm0.0029 | 0.6604\pm0.0010 | 0.6674\pm0.0061 | 1.1882 \pm 0.0199 | 1.1739 \pm 0.0118 | 1.1619\pm0.0203 |
| | Federated | FedAvg [1] | 0.6446 \pm 0.0059 | 0.6476 \pm 0.0011 | 0.6585 \pm 0.0039 | 1.2960 \pm 0.0274 | 1.2853 \pm 0.0204 | 1.2816 \pm 0.0118 |
| | | AFA-CD [13] | 0.6521 \pm 0.0055 | 0.6560 \pm 0.0031 | 0.6583 \pm 0.0058 | 1.2229 \pm 0.0251 | 1.2279 \pm 0.0301 | 1.2318 \pm 0.0151 |
| | | FedNova [12] | 0.6439 \pm 0.0041 | 0.6495 \pm 0.0037 | 0.6594 \pm 0.0048 | 1.3333 \pm 0.0801 | 1.2910 \pm 0.0127 | 1.2768 \pm 0.0231 |
| | | FedProx [11] | 0.6245 \pm 0.0046 | 0.6331 \pm 0.0028 | 0.6405 \pm 0.0036 | 1.1131\pm0.0137 | 1.0968\pm0.0100 | 1.4779 \pm 0.0139 |
| | | FedDisco [14] | 0.6466 \pm 0.0074 | 0.6535 \pm 0.0045 | 0.6560 \pm 0.0024 | 1.3282 \pm 0.0385 | 1.3158 \pm 0.0221 | 1.2983 \pm 0.0139 |
| | | SCAFFOLD [10] | 0.6460 \pm 0.0014 | 0.6535 \pm 0.0035 | 0.6587 \pm 0.0062 | 1.3284 \pm 0.0220 | 1.3082 \pm 0.0182 | 1.2957 \pm 0.0289 |
| Fashion-MNIST | Central | SGD | 0.9047 \pm 0.0017 | 0.9063 \pm 0.0009 | 0.9045 \pm 0.0007 | 0.2964 \pm 0.0056 | 0.2979 \pm 0.0140 | 0.2870 \pm 0.0031 |
| | | OSAFL (Ours) | 0.8949\pm0.0022 | 0.8974\pm0.0020 | 0.8983 \pm 0.0013 | 0.3412\pm0.0111 | 0.3357 \pm 0.0048 | 0.3247 \pm 0.0047 |
| | Federated | FedAvg [1] | 0.8897 \pm 0.0027 | 0.8926 \pm 0.0014 | 0.8965 \pm 0.0004 | 0.3630 \pm 0.0111 | 0.3585 \pm 0.0087 | 0.3592 \pm 0.0037 |
| | | AFA-CD [13] | 0.8933 \pm 0.0022 | 0.8972 \pm 0.0019 | 0.8986\pm0.0009 | 0.3441 \pm 0.0086 | 0.3388 \pm 0.0070 | 0.3367 \pm 0.0065 |
| | | FedNova [12] | 0.8914 \pm 0.0028 | 0.8952 \pm 0.0022 | 0.8961 \pm 0.0008 | 0.3561 \pm 0.0105 | 0.3553 \pm 0.0140 | 0.3572 \pm 0.0032 |
| | | FedProx [11] | 0.8786 \pm 0.0033 | 0.8809 \pm 0.0014 | 0.8845 \pm 0.0013 | 0.3425 \pm 0.0075 | 0.3325\pm0.0030 | 0.3243\pm0.0034 |
| | | FedDisco [14] | 0.8915 \pm 0.0020 | 0.8950 \pm 0.0007 | 0.8979 \pm 0.0016 | 0.3708 \pm 0.0117 | 0.3559 \pm 0.0058 | 0.3576 \pm 0.0031 |
| | | SCAFFOLD [10] | 0.8914 \pm 0.0019 | 0.8947 \pm 0.0008 | 0.8970 \pm 0.0013 | 0.3678 \pm 0.0094 | 0.3610 \pm 0.0058 | 0.3610 \pm 0.0060 |
| MNIST | Central | SGD | 0.9901 \pm 0.0005 | 0.9912 \pm 0.0010 | 0.9906 \pm 0.0007 | 0.0368 \pm 0.0033 | 0.0317 \pm 0.0039 | 0.0358 \pm 0.0026 |
| | | OSAFL (Ours) | 0.9881\pm0.0010 | 0.9892\pm0.0008 | 0.9896 \pm 0.0007 | 0.0374\pm0.0029 | 0.0362\pm0.0022 | 0.0361 \pm 0.0020 |
| | Federated | FedAvg [1] | 0.9881\pm0.0006 | 0.9884 \pm 0.0003 | 0.9893 \pm 0.0007 | 0.0403 \pm 0.0014 | 0.0364 \pm 0.0013 | 0.0350 \pm 0.0015 |
| | | AFA-CD [13] | 0.9855 \pm 0.0018 | 0.9880 \pm 0.0021 | 0.9890 \pm 0.0003 | 0.0458 \pm 0.0070 | 0.0392 \pm 0.0045 | 0.0368 \pm 0.0011 |
| | | FedNova [12] | 0.9878 \pm 0.0007 | 0.9884 \pm 0.0004 | 0.9898\pm0.0004 | 0.0394 \pm 0.0010 | 0.0375 \pm 0.0020 | 0.0339\pm0.0026 |
| | | FedProx [11] | 0.9853 \pm 0.0003 | 0.9862 \pm 0.0007 | 0.9870 \pm 0.0005 | 0.0447 \pm 0.0011 | 0.0432 \pm 0.0023 | 0.0396 \pm 0.0013 |
| | | FedDisco [14] | 0.9881\pm0.0002 | 0.9886 \pm 0.0006 | 0.9891 \pm 0.0009 | 0.0388 \pm 0.0012 | 0.0381 \pm 0.0010 | 0.0357 \pm 0.0029 |
| | | SCAFFOLD [10] | 0.9877 \pm 0.0004 | 0.9885 \pm 0.0002 | 0.9898\pm0.0007 | 0.0386 \pm 0.0014 | 0.0376 \pm 0.0019 | 0.0346 \pm 0.0018 |

ples can appear from only a few labels. As such, FIFO deletion policy may not be ideal since this policy does not consider the label distribution in the dataset and simply removes the oldest training sample. As such, a few rare samples can be deleted and lost forever. Intuitively, one should retain the samples in such a way that reduces the label skewness. Therefore, TrimTopLabel policy can help to tame the label skewness in the training datasets. However, the training is still challenging since once a training sample is deleted, it does not reappear.

The simulation results in Figs. 5 - 8 show the performance comparisons using both data deletion policies. These results suggest some fluctuations with both data deletion policies in all datasets. We observe that the FL algorithms have some performance deviations from the centralized SGD performance, which is like the video caching task, expected since all training samples are not available in FL. It is worth noting that we also observe high fluctuations with the centralized SGD algorithm, even though we assume all training samples are centrally available. These happen for two main reasons: (a) the dynamic dataset of each client contributes to a time-varying central dataset since $\mathcal{D}^t = \bigcup_{u=0}^{U-1} \mathcal{D}_u^t$ in this case, and (b) the results show the performance in every SGD step compared to the FL algorithms where each client performs κ_u^t SGD steps in every global round t . Besides, in both data deletion policies, the test accuracies are quite similar for the FL algorithms except for FedProx. However, FedProx delivers the lowest test loss on the CIFAR-10 dataset. For example, for FIFO policy with Dir ($\alpha = 0.9$) on CIFAR 10 dataset, the test accuracies at the 150th global round are 66.73%, 64.39%, 64.07%, 64.14%, 64.25%, 60.43%, 63.61%, 63.94%, respectively, for centralized SGD, OSAFL, FedAvg, AFA, FedNova, FedProx, FedProx, FedDisco and SCAFFOLD, respectively, while the test losses are 1.01, 1.17, 1.30, 1.23, 1.28, 1.14, 1.33, 1.29,

respectively. Besides, when TrimTopLabel data deletion policy is used, the test accuracies are 66.33%, 64.66%, 64.28%, 64.63%, 64.22%, 61.13%, 64.31% and 64.22%, while the test losses are 1.03, 1.18, 1.32, 1.23, 1.3, 1.13, 1.31 and 1.31, respectively, for the above algorithms. The above findings suggest that TrimTopLabel data deletion policy yields slightly higher test accuracies than the FIFO policy for all 7 FL algorithms.

While Figs. 5 - 8 show the performance comparisons for the symmetric Dirichlet parameter $\alpha = 0.9$, we also consider other values and report the best test accuracy and loss for all baselines in Table II and Table III, respectively for FIFO and TrimTopLabel policies. From the results, it is evident that, in all cases, a high α gives better performance since a high α value ensures less skewness in label distributions. Besides, our proposed OSAFL has the best test accuracies on CIFAR-10 and second best test losses for all considered α values. Furthermore, OSAFL has either the best or second best performance for all cases except the test loss for the MNIST dataset with TrimTopLabel policy and $\alpha = 10$. As such, on balance, our proposed OSAFL algorithm performs relatively well compared to other FL baselines.

V. CONCLUSION

In this paper, we proposed a new algorithm called OSAFL to tame resource constraints in wireless networks. Our extensive theoretical analysis suggested optimizing the *scores* of the clients for global model aggregation in order to facilitate the proposed algorithm's convergence. Furthermore, due to the fractional objective function and non-convex nature of the original optimization problem, we considered a sub-optimal strategy, which suggested that the *scores* are proportional to the gradient similarities between the client's local gradient and accumulated local gradients from all clients. Moreover,

our extensive simulation results validated the effectiveness of the proposed OS AFL algorithm in two different tasks on six different datasets with four different ML models.

ACKNOWLEDGMENT

The authors acknowledge the Center for Advanced Research Computing (CARC) at the University of Southern California for providing computing resources that have contributed to the research. URL: <https://carc.usc.edu>.

REFERENCES

- [1] B. McMahan, E. Moore, D. Ramage, S. Hampson, and B. A. y. Arcas, "Communication-Efficient Learning of Deep Networks from Decentralized Data," in *Proc. AISTAT*, vol. 54. PMLR, 20–22 Apr 2017, pp. 1273–1282. [Online]. Available: <https://proceedings.mlr.press/v54/mcmahan17a.html>
- [2] S. Niknam, H. S. Dhillon, and J. H. Reed, "Federated learning for wireless communications: Motivation, opportunities, and challenges," *IEEE Commun. Magaz.*, vol. 58, no. 6, pp. 46–51, 2020.
- [3] M. F. Pervej, A. F. Molisch, "Resource-aware hierarchical federated learning in wireless video caching networks," *arXiv preprint arXiv:2402.04216*, 2024.
- [4] S. Hosseinalipour, S. Wang, N. Michelusi, V. Aggarwal, C. G. Brinton, D. J. Love, and M. Chiang, "Parallel successive learning for dynamic distributed model training over heterogeneous wireless networks," *IEEE/ACM Trans. Network.*, vol. 32, no. 1, pp. 222–237, 2024.
- [5] M. F. Pervej, J. Guo, K. J. Kim, K. Parsons, P. Orlik, S. Di Cairano, M. Menner, K. Berntorp, Y. Nagai, and H. Dai, "Mobility, communication and computation aware federated learning for internet of vehicles," in *Proc. IEEE Intel. Vehicles Symp.*, 2022, pp. 750–757.
- [6] N. Chen, Z. Cheng, X. Fan, Z. Liu, B. Huang, Y. Zhao, L. Huang, X. Du, and M. Guizani, "Integrated sensing, communication, and computing for cost-effective multimodal federated perception," *ACM Trans. Multimedia Comput. Commun. App.*, vol. 20, no. 8, pp. 1–28, 2024.
- [7] C. Luo, J. Ji, Q. Wang, X. Chen, and P. Li, "Channel state information prediction for 5g wireless communications: A deep learning approach," *IEEE Trans. Network Sci. Engg.*, vol. 7, no. 1, pp. 227–236, 2018.
- [8] L. Bottou, F. E. Curtis, and J. Nocedal, "Optimization methods for large-scale machine learning," *SIAM review*, vol. 60, no. 2, pp. 223–311, 2018.
- [9] A. Krizhevsky, "Learning multiple layers of features from tiny images," *Master's Thesis, University of Toronto*, 2009. [Online]. Available: <https://www.cs.toronto.ca/~kriz/learning-features-2009-TR.pdf>
- [10] S. P. Karimireddy, S. Kale, M. Mohri, S. Reddi, S. Stich, and A. T. Suresh, "SCAFFOLD: Stochastic controlled averaging for federated learning," in *Proc. ICML*, vol. 119. PMLR, 13–18 Jul 2020, pp. 5132–5143. [Online]. Available: <https://proceedings.mlr.press/v119/karimireddy20a.html>
- [11] T. Li, A. K. Sahu, M. Zaheer, M. Sanjabi, A. Talwalkar, and V. Smith, "Federated optimization in heterogeneous networks," vol. 2, pp. 429–450, 2020. [Online]. Available: https://proceedings.mlsys.org/paper_files/paper/2020/file/1f5fe83998a09396e6e6477d9475ba0c-Paper.pdf
- [12] J. Wang, Q. Liu, H. Liang, G. Joshi, and H. V. Poor, "Tackling the objective inconsistency problem in heterogeneous federated optimization," in *Proc. NeurIPS*, vol. 33. Curran Associates, Inc., 2020, pp. 7611–7623. [Online]. Available: https://proceedings.neurips.cc/paper_files/paper/2020/file/564127c03caab942e503ee6f810f54fd-Paper.pdf
- [13] H. Yang, X. Zhang, P. Khanduri, and J. Liu, "Anarchic federated learning," in *Proc. ICML*, vol. 162. PMLR, 17–23 Jul 2022, pp. 25 331–25 363. [Online]. Available: <https://proceedings.mlr.press/v162/yang22r.html>
- [14] R. Ye, M. Xu, J. Wang, C. Xu, S. Chen, and Y. Wang, "FedDisco: Federated learning with discrepancy-aware collaboration," in *Proc. ICML*, vol. 202. PMLR, 23–29 Jul 2023, pp. 39 879–39 902. [Online]. Available: <https://proceedings.mlr.press/v202/ye23f.html>
- [15] M. Chen, Z. Yang, W. Saad, C. Yin, H. V. Poor, and S. Cui, "A joint learning and communications framework for federated learning over wireless networks," *IEEE Trans. Wireless Commun.*, vol. 20, no. 1, pp. 269–283, 2020.
- [16] M. M. Amiri and D. Gündüz, "Federated learning over wireless fading channels," *IEEE Trans. Wireless Commun.*, vol. 19, no. 5, pp. 3546–3557, 2020.
- [17] N. H. Tran, W. Bao, A. Zomaya, M. N. Nguyen, and C. S. Hong, "Federated learning over wireless networks: Optimization model design and analysis," in *Proc. IEEE INFOCOM*. IEEE, 2019, pp. 1387–1395.
- [18] M. F. Pervej, R. Jin, and H. Dai, "Resource constrained vehicular edge federated learning with highly mobile connected vehicles," *IEEE J. Sel. Areas Commun.*, vol. 41, no. 6, pp. 1825–1844, 2023.
- [19] X. Zhou, J. Zhao, H. Han, and C. Guet, "Joint optimization of energy consumption and completion time in federated learning," in *Proc. IEEE ICDCS*, 2022, pp. 1005–1017.
- [20] Z. Zhao, J. Wang, W. Hong, T. Q. S. Quek, Z. Ding, and M. Peng, "Ensemble federated learning with non-iid data in wireless networks," *IEEE Trans. Wireless Commun.*, vol. 23, no. 4, pp. 3557–3571, 2024.
- [21] B. Li, J. Perazzone, A. Swami, and S. Segarra, "Learning to transmit with provable guarantees in wireless federated learning," *IEEE Trans. Wireless Commun.*, vol. 23, no. 7, pp. 7439–7455, 2024.
- [22] Y.-J. Liu, S. Qin, Y. Sun, and G. Feng, "Resource consumption for supporting federated learning in wireless networks," *IEEE Trans. Wireless Commun.*, vol. 21, no. 11, pp. 9974–9989, 2022.
- [23] J. Zhang, S. Chen, X. Zhou, X. Wang, and Y.-B. Lin, "Joint scheduling of participants, local iterations, and radio resources for fair federated learning over mobile edge networks," *IEEE Trans. Mobile Comput.*, vol. 22, no. 7, pp. 3985–3999, 2023.
- [24] R. Saha, S. Misra, A. Chakraborty, C. Chatterjee, and P. K. Deb, "Data-centric client selection for federated learning over distributed edge networks," *IEEE Trans. Parallel Distrib. Sys.*, vol. 34, no. 2, pp. 675–686, 2022.
- [25] J. Yao, Z. Yang, W. Xu, M. Chen, and D. Niyato, "Gomore: Global model reuse for resource-constrained wireless federated learning," *IEEE Wireless Commun. Lett.*, vol. 12, no. 9, pp. 1543–1547, 2023.
- [26] Z. Chen, W. Yi, H. Shin, A. Nallanathan, and G. Y. Li, "Efficient wireless federated learning with partial model aggregation," *IEEE Trans. Commun.*, 2024.
- [27] Z. Liu, M. Sun, T. Zhou, G. Huang, and T. Darrell, "Rethinking the value of network pruning," *arXiv preprint arXiv:1810.05270*, 2018.
- [28] A. Polino, R. Pascanu, and D. Alistarh, "Model compression via distillation and quantization," in *Proc. ICLR*, 2018. [Online]. Available: <https://openreview.net/forum?id=S1XolQBRW>
- [29] Z. Chen, W. Yi, H. Shin, and A. Nallanathan, "Adaptive model pruning for communication and computation efficient wireless federated learning," *IEEE Trans. Wireless Commun.*, vol. 23, no. 7, pp. 7582–7598, 2024.
- [30] M. F. Pervej, R. Jin, and H. Dai, "Hierarchical federated learning in wireless networks: Pruning tackles bandwidth scarcity and system heterogeneity," *IEEE Trans. Wireless Commun.*, 2024.
- [31] S. Wang, M. Chen, C. G. Brinton, C. Yin, W. Saad, and S. Cui, "Performance optimization for variable bandwidth federated learning in wireless networks," *IEEE Trans. Wireless Commun.*, vol. 23, no. 3, pp. 2340–2356, 2024.
- [32] M. Kim, W. Saad, M. Mozaffari, and M. Debbah, "Green, quantized federated learning over wireless networks: An energy-efficient design," *IEEE Trans. Wireless Commun.*, vol. 23, no. 2, pp. 1386–1402, 2024.
- [33] S. Wang, T. Tuor, T. Salonidis, K. K. Leung, C. Makaya, T. He, and K. Chan, "Adaptive federated learning in resource constrained edge computing systems," *IEEE J. Sel. Areas Commun.*, vol. 37, no. 6, pp. 1205–1221, 2019.
- [34] H. Yang, M. Fang, and J. Liu, "Achieving linear speedup with partial worker participation in non-IID federated learning," in *Proc. ICLR*, 2021. [Online]. Available: <https://openreview.net/forum?id=jDdzh5ul-d>
- [35] S. P. Boyd and L. Vandenberghe, *Convex optimization*. Cambridge university press, 2004.
- [36] H. Xiao, K. Rasul, and R. Vollgraf, "Fashion-mnist: a novel image dataset for benchmarking machine learning algorithms," *arXiv preprint arXiv:1708.07747*, 2017.
- [37] Y. LeCun, C. Cortes, and C. Burges, "Mnist handwritten digit database," *ATT Labs*, vol. 2, 2010. [Online]. Available: yann.lecun.com/exdb/mnist

SUPPLEMENTARY MATERIALS

A. Key Equations

Each client have the following local objective

$$f_u(\mathbf{w}|\mathcal{D}_u^t) := \frac{1}{|\mathcal{D}_u^t|} \sum_{(\mathbf{x},y) \in \mathcal{D}_u^t} l(\mathbf{w}|(\mathbf{x},y)), \quad (32)$$

where $l(\mathbf{w}|(\mathbf{x},y))$ is the loss associated to training sample (\mathbf{x},y) and \mathcal{D}_u^t is the available training dataset of client u during global round t .

Upon receiving the global model \mathbf{w}^t from the central server (CS), the clients synchronize their local models $\mathbf{w}_u^{t,0} \leftarrow \mathbf{w}^t$ and take $\kappa_u^t \in [1, \kappa]$ number of local stochastic gradient descent (SGD) steps

$$\mathbf{w}_u^{t,\kappa_u^t} = \mathbf{w}_u^{t,0} - \eta \sum_{\tau=0}^{\kappa_u^t-1} g_u(\mathbf{w}_u^{t,\tau}|\mathcal{D}_u^t), \quad (33)$$

where η is the learning rate.

Upon finishing the local training, the clients offload normalized accumulated gradients

$$\mathbf{d}_u^t := \frac{1}{\kappa_u^t} \sum_{\tau=0}^{\kappa_u^t-1} g_u(\mathbf{w}_u^{t,\tau}|\mathcal{D}_u^t) = \frac{\mathbf{w}_u^{t,0} - \mathbf{w}_u^{t,\kappa_u^t}}{\eta \kappa_u^t} \quad (34)$$

The CS takes a global SGD step with step size $\tilde{\eta}$ using the normalized accumulated gradients as

$$\mathbf{w}^{t+1} = \mathbf{w}^t - \tilde{\eta} \eta \sum_{u=0}^{U-1} \alpha_u \tilde{\mathbf{d}}_u^t, \quad (35)$$

where $\tilde{\mathbf{d}}_u^t := \Delta_u^t \mathbf{d}_u^t$ and Δ_u^t is the *score* of client u during time t . Using the convergence bound we optimize this *score* and find that

$$\begin{aligned} \Delta_u^t &\propto \text{Constant} + \left[\frac{C_1}{2\beta\tilde{\eta}\sigma^2\alpha_u^2 + C_1} \right] \lambda_u^t \\ &\propto \lambda_u^t = \exp \left[\frac{\langle \mathbf{d}^t, \mathbf{d}_u^t \rangle}{\|\mathbf{d}^t\|_2 \cdot \|\mathbf{d}_u^t\|_2} \right], \end{aligned} \quad (36)$$

where $\mathbf{d}^t := \frac{1}{U} \sum_{u=0}^{U-1} \mathbf{d}_u^t$ and $C_1 = 8\beta^2\eta^2(\sigma^2 + 3\kappa\varepsilon^2)\alpha_u\kappa_u^t + 24\psi\beta^2\eta^2\kappa^2\alpha_u$.

The proposed online-score-aided federated learning (OSAF_L) thus has the following global objective function.

$$f(\mathbf{w}^t|\mathcal{D}^t) := \sum_{u=0}^{U-1} \alpha_u \Delta_u^t f_u(\mathbf{w}^t|\mathcal{D}_u^t) \quad (37)$$

For brevity and notational simplicity, we represent the local loss function $f_u(\mathbf{w}|\mathcal{D}_u^t)$ by $f_u(\mathbf{w})$ and the global loss function $f(\mathbf{w}|\mathcal{D}^t)$ by $f(\mathbf{w})$ for the rest of the manuscript. Similarly, the stochastic gradient $g_u(\mathbf{w}|\mathcal{D}_u^t)$ and the true gradient $\nabla f_u(\mathbf{w}|\mathcal{D}_u^t)$ are succinctly denoted by $g_u(\mathbf{w})$ and $\nabla f_u(\mathbf{w})$, respectively. In an federated learning (FL) round t , we should interpret $f_u(\mathbf{w})$ and its gradients $g_u(\mathbf{w})$ and $\nabla f(\mathbf{w})$ to be dependent on the available datasets \mathcal{D}_u^t , while the global loss function and its gradient depend on \mathcal{D}^t .

B. Key Assumptions

We make the following standard assumptions [12], [13], [14], [18], [30] that are needed for the theoretical analysis.

Assumption 1 (Smoothness). *The local loss functions are β -Lipschitz smooth. That is, for some $\beta > 0$, $\|\nabla f_u(\mathbf{w}) - \nabla f_u(\mathbf{w}')\| \leq \beta\|\mathbf{w} - \mathbf{w}'\|$, for all $\mathbf{w}, \mathbf{w}' \in \mathbb{R}^N$ and $u \in \mathcal{U}$.*

Assumption 2 (Unbiased gradient with bounded variance). *The stochastic gradient at each client is an unbiased estimate of the client's true gradient, i.e., $\mathbb{E}_{\zeta \sim \mathcal{D}_u^t} [g_u(\mathbf{w})] = \nabla f_u(\mathbf{w})$, where $\mathbb{E}[\cdot]$ is the expectation operator. Besides, the stochastic gradient has a bounded variance, i.e., $\mathbb{E}_{\zeta \sim \mathcal{D}_u^t} [\|g_u(\mathbf{w}) - \nabla f_u(\mathbf{w})\|^2] \leq \sigma^2$, for some $\sigma \geq 0$ and for all $u \in \mathcal{U}$.*

Assumption 3 (Bounded gradient divergence). *The divergence between the local and global gradients is bounded, i.e., $\|\nabla f_u(\mathbf{w}) - \nabla f(\mathbf{w})\|^2 \leq \varepsilon^2$, for some $\varepsilon \geq 0$ and $u \in \mathcal{U}$.*

While assumptions 1 and 2 are standard and widely used for the theoretical analysis of SGD [8], assumption 3 is widely used for the convergence analysis of FL [13], [33].

APPENDIX A
PROOF OF THEOREM 1

Theorem 1. Suppose the above assumptions hold. When the learning rates satisfy $\eta\tilde{\eta} \leq \frac{1}{\beta}$ and $\eta < \frac{1}{\sqrt{6\beta\kappa}}$, we have

$$\frac{1}{T} \sum_{t=0}^{T-1} \mathbb{E} \|\nabla f(\mathbf{w}^t)\|^2 \leq \frac{1}{T} \sum_{t=0}^{T-1} \left\{ \frac{1}{A^t} \left[\frac{2F^t}{\eta\tilde{\eta}} + \beta\eta\tilde{\eta}\sigma^2 \sum_{u=0}^{U-1} \alpha_u^2 (\Delta_u^t)^2 + 4\beta^2\eta^2\sigma^2 \sum_{u=0}^{U-1} \alpha_u \kappa_u^t B_u^t + 12\beta^2\eta^2\epsilon^2 \sum_{u=0}^{U-1} \alpha_u B_u^t (\kappa_u^t)^2 \right] \right\}, \quad (38)$$

where $F^t = \mathbb{E}[f(\mathbf{w}^t)] - \mathbb{E}[f(\mathbf{w}^{t+1})]$, $A^t = 1 - 12\beta^2\eta^2\kappa^2 \sum_{u=0}^{U-1} \alpha_u B_u^t$ and $B_u^t = (\Delta_u^t)^2 - 2\Delta_u^t \lambda_u^t + 2(\lambda_u^t)^2$.

Proof. For convenience, we denote

$$\tilde{\mathbf{d}}_u^t := \Delta_u^t \mathbf{d}_u^t = \Delta_u^t \frac{1}{\kappa_u^t} \sum_{\tau=0}^{\kappa_u^t-1} g_u(\mathbf{w}_u^{t,\tau}) \quad (39)$$

$$\tilde{\mathbf{h}}_u^t := \Delta_u^t \mathbf{h}_u^t = \Delta_u^t \frac{1}{\kappa_u^t} \sum_{\tau=0}^{\kappa_u^t-1} \nabla f_u(\mathbf{w}_u^{t,\tau}) \quad (40)$$

Using the aggregation rule defined in (35), we write

$$\begin{aligned} f(\mathbf{w}^{t+1}) &= f(\mathbf{w}^t - \eta\tilde{\eta} \sum_{u=0}^{U-1} \alpha_u \tilde{\mathbf{d}}_u^t) \\ &\stackrel{(a)}{\leq} f(\mathbf{w}^t) - \left\langle \nabla f(\mathbf{w}^t), \eta\tilde{\eta} \sum_{u=0}^{U-1} \alpha_u \tilde{\mathbf{d}}_u^t \right\rangle + \frac{\beta\eta^2\tilde{\eta}^2}{2} \left\| \sum_{u=0}^{U-1} \alpha_u \tilde{\mathbf{d}}_u^t \right\|^2, \end{aligned} \quad (41)$$

where (a) stems from the β -smoothness property.

Now, we write the following by taking expectation on both sides.

$$\mathbb{E}[f(\mathbf{w}^{t+1})] = \mathbb{E}[f(\mathbf{w}^t)] - \eta\tilde{\eta} \underbrace{\mathbb{E} \left[\left\langle \nabla f(\mathbf{w}^t), \sum_{u=0}^{U-1} \alpha_u \tilde{\mathbf{d}}_u^t \right\rangle \right]}_{\mathbf{T}_1} + \underbrace{\frac{\beta\eta^2\tilde{\eta}^2}{2} \mathbb{E} \left[\left\| \sum_{u=0}^{U-1} \alpha_u \tilde{\mathbf{d}}_u^t \right\|^2 \right]}_{\mathbf{T}_2}. \quad (42)$$

We simplify \mathbf{T}_1 as

$$\begin{aligned} \mathbf{T}_1 &= \mathbb{E} \left[\left\langle \nabla f(\mathbf{w}^t), \sum_{u=0}^{U-1} \alpha_u \tilde{\mathbf{d}}_u^t + \sum_{u=0}^{U-1} \alpha_u \tilde{\mathbf{h}}_u^t - \sum_{u=0}^{U-1} \alpha_u \tilde{\mathbf{h}}_u^t \right\rangle \right] \\ &= \mathbb{E} \left[\left\langle \nabla f(\mathbf{w}^t), \sum_{u=0}^{U-1} \alpha_u \tilde{\mathbf{d}}_u^t - \sum_{u=0}^{U-1} \alpha_u \tilde{\mathbf{h}}_u^t \right\rangle \right] + \mathbb{E} \left[\left\langle \nabla f(\mathbf{w}^t), \sum_{u=0}^{U-1} \alpha_u \tilde{\mathbf{h}}_u^t \right\rangle \right] \\ &= \mathbb{E} \left[\left\langle \nabla f(\mathbf{w}^t), \sum_{u=0}^{U-1} \alpha_u \Delta_u^t [\mathbf{d}_u^t - \mathbf{h}_u^t] \right\rangle \right] + \mathbb{E} \left[\left\langle \nabla f(\mathbf{w}^t), \sum_{u=0}^{U-1} \alpha_u \tilde{\mathbf{h}}_u^t \right\rangle \right] \\ &= \mathbb{E} \left[\left\langle \nabla f(\mathbf{w}^t), \sum_{u=0}^{U-1} \alpha_u \Delta_u^t \frac{1}{\kappa_u^t} \sum_{\tau=0}^{\kappa_u^t-1} [g_u(\mathbf{w}_u^{t,\tau}) - \nabla f_u(\mathbf{w}_u^{t,\tau})] \right\rangle \right] + \mathbb{E} \left[\left\langle \nabla f(\mathbf{w}^t), \sum_{u=0}^{U-1} \alpha_u \tilde{\mathbf{h}}_u^t \right\rangle \right] \\ &\stackrel{(a)}{=} \mathbb{E} \left[\left\langle \nabla f(\mathbf{w}^t), \sum_{u=0}^{U-1} \alpha_u \tilde{\mathbf{h}}_u^t \right\rangle \right] \\ &\stackrel{(b)}{=} \frac{1}{2} \mathbb{E} \|\nabla f(\mathbf{w}^t)\|^2 + \frac{1}{2} \mathbb{E} \left\| \sum_{u=0}^{U-1} \alpha_u \tilde{\mathbf{h}}_u^t \right\|^2 - \frac{1}{2} \mathbb{E} \left\| \nabla f(\mathbf{w}^t) - \sum_{u=0}^{U-1} \alpha_u \tilde{\mathbf{h}}_u^t \right\|^2, \end{aligned} \quad (43)$$

where (a) stems from assumption 2, i.e., $\mathbb{E}[g_u(\mathbf{w}_u^{t,\tau})] = \nabla f_u(\mathbf{w}_u^{t,\tau})$ and (b) comes from the fact that $\|\mathbf{x} - \mathbf{y}\|^2 = \|\mathbf{x}\|^2 + \|\mathbf{y}\|^2 - 2\langle \mathbf{x}, \mathbf{y} \rangle$.

Simplify \mathbf{T}_2 as

$$\begin{aligned} \mathbf{T}_2 &= \frac{\beta\eta^2\tilde{\eta}^2}{2} \mathbb{E} \left[\left\| \sum_{u=0}^{U-1} \alpha_u \tilde{\mathbf{d}}_u^t \right\|^2 \right] \\ &\stackrel{(a)}{=} \frac{\beta\eta^2\tilde{\eta}^2}{2} \left\{ \mathbb{E} \left[\left\| \sum_{u=0}^{U-1} \alpha_u \tilde{\mathbf{d}}_u^t - \mathbb{E} \left[\sum_{u=0}^{U-1} \alpha_u \tilde{\mathbf{d}}_u^t \right] \right\|^2 \right] + \left(\mathbb{E} \left[\sum_{u=0}^{U-1} \alpha_u \tilde{\mathbf{d}}_u^t \right] \right)^2 \right\} \\ &= \frac{\beta\eta^2\tilde{\eta}^2}{2} \left\{ \mathbb{E} \left[\left\| \sum_{u=0}^{U-1} \alpha_u \tilde{\mathbf{d}}_u^t - \sum_{u=0}^{U-1} \alpha_u \tilde{\mathbf{h}}_u^t \right\|^2 \right] + \left\| \sum_{u=0}^{U-1} \alpha_u \tilde{\mathbf{h}}_u^t \right\|^2 \right\} \\ &= \frac{\beta\eta^2\tilde{\eta}^2}{2} \left\{ \mathbb{E} \left[\left\| \sum_{u=0}^{U-1} \alpha_u \frac{\Delta_u^t}{\kappa_u^t} \sum_{\tau=0}^{\kappa_u^t-1} (g_u(\mathbf{w}_u^{t,\tau}) - \nabla f_u(\mathbf{w}_u^{t,\tau})) \right\|^2 \right] + \left\| \sum_{u=0}^{U-1} \alpha_u \tilde{\mathbf{h}}_u^t \right\|^2 \right\} \\ &\stackrel{(b)}{=} \frac{\beta\eta^2\tilde{\eta}^2}{2} \sum_{u=0}^{U-1} \alpha_u^2 \mathbb{E} \left[\left\| \frac{\Delta_u^t}{\kappa_u^t} \sum_{\tau=0}^{\kappa_u^t-1} (g_u(\mathbf{w}_u^{t,\tau}) - \nabla f_u(\mathbf{w}_u^{t,\tau})) \right\|^2 \right] + \frac{\beta\eta^2\tilde{\eta}^2}{2} \left\| \sum_{u=0}^{U-1} \alpha_u \tilde{\mathbf{h}}_u^t \right\|^2 \\ &\stackrel{(c)}{\leq} \frac{\beta\eta^2\tilde{\eta}^2}{2} \sum_{u=0}^{U-1} \alpha_u^2 \frac{(\Delta_u^t)^2}{\kappa_u^t} \sum_{\tau=0}^{\kappa_u^t-1} \left\{ \mathbb{E} \left[\left\| g_u(\mathbf{w}_u^{t,\tau}) - \nabla f_u(\mathbf{w}_u^{t,\tau}) \right\|^2 \right] + \frac{\beta\eta^2\tilde{\eta}^2}{2} \left\| \sum_{u=0}^{U-1} \alpha_u \tilde{\mathbf{h}}_u^t \right\|^2 \right\} \\ &\stackrel{(d)}{\leq} \frac{\beta\eta^2\tilde{\eta}^2\sigma^2}{2} \sum_{u=0}^{U-1} \alpha_u^2 (\Delta_u^t)^2 + \frac{\beta\eta^2\tilde{\eta}^2}{2} \left\| \sum_{u=0}^{U-1} \alpha_u \tilde{\mathbf{h}}_u^t \right\|^2, \end{aligned} \quad (44)$$

where we used the definition of variance in (a). Besides, (b) stems from the unbiased stochastic gradients assumption and the independence of the stochastic gradients. Furthermore, (c) is true since $\|\sum_{i=1}^I \mathbf{x}_i\|^2 \leq I\|\mathbf{x}_i\|^2$. Finally, (d) appears from the bounded variance of the gradients assumption.

Plugging T_1 and T_2 in (42), and taking expectation on both sides, we get

$$\begin{aligned} \mathbb{E}[f(\mathbf{w}^{t+1})] &\leq \mathbb{E}[f(\mathbf{w}^t)] - \frac{\eta\tilde{\eta}}{2}\mathbb{E}\|\nabla f(\mathbf{w}^t)\|^2 - \frac{\eta\tilde{\eta}}{2}\mathbb{E}\left\|\sum_{u=0}^{U-1}\alpha_u\tilde{\mathbf{h}}_u\right\|^2 + \frac{\eta\tilde{\eta}}{2}\mathbb{E}\left\|\nabla f(\mathbf{w}^t) - \sum_{u=0}^{U-1}\alpha_u\tilde{\mathbf{h}}_u\right\|^2 + \\ &\quad \frac{\beta\eta^2\tilde{\eta}^2\sigma^2}{2}\sum_{u=0}^{U-1}\alpha_u^2(\Delta_u^t)^2 + \frac{\beta\eta^2\tilde{\eta}^2}{2}\mathbb{E}\left\|\sum_{u=0}^{U-1}\alpha_u\tilde{\mathbf{h}}_u\right\|^2 \\ &= \mathbb{E}[f(\mathbf{w}^t)] - \frac{\eta\tilde{\eta}}{2}\mathbb{E}\|\nabla f(\mathbf{w}^t)\|^2 + \frac{\beta\eta^2\tilde{\eta}^2\sigma^2}{2}\sum_{u=0}^{U-1}\alpha_u^2(\Delta_u^t)^2 + \frac{\eta\tilde{\eta}}{2}\mathbb{E}\left\|\nabla f(\mathbf{w}^t) - \sum_{u=0}^{U-1}\alpha_u\tilde{\mathbf{h}}_u\right\|^2 - \frac{\eta\tilde{\eta}}{2}(1-\beta\eta\tilde{\eta})\mathbb{E}\left\|\sum_{u=0}^{U-1}\alpha_u\tilde{\mathbf{h}}_u\right\|^2, \end{aligned} \quad (45)$$

When $\eta\tilde{\eta} \leq \frac{1}{\beta}$, we have $(1-\beta\eta\tilde{\eta}) \geq 0$. Therefore, we drop the last term, which yields

$$\mathbb{E}[f(\mathbf{w}^{t+1})] - \mathbb{E}[f(\mathbf{w}^t)] \leq -\frac{\eta\tilde{\eta}}{2}\mathbb{E}\|\nabla f(\mathbf{w}^t)\|^2 + \frac{\beta\eta^2\tilde{\eta}^2\sigma^2}{2}\sum_{u=0}^{U-1}\alpha_u^2(\Delta_u^t)^2 + \underbrace{\frac{\eta\tilde{\eta}}{2}\mathbb{E}\left\|\nabla f(\mathbf{w}^t) - \sum_{u=0}^{U-1}\alpha_u\tilde{\mathbf{h}}_u\right\|^2}_{T_3}. \quad (46)$$

Simplify T_3 as

$$\begin{aligned} T_3 &= \mathbb{E}\left[\left\|\nabla f(\mathbf{w}^t) - \sum_{u=0}^{U-1}\alpha_u\tilde{\mathbf{h}}_u\right\|^2\right] = \mathbb{E}\left[\left\|\sum_{u=0}^{U-1}\alpha_u\Delta_u^t\nabla f_u(\mathbf{w}^t) - \sum_{u=0}^{U-1}\alpha_u\Delta_u^t\mathbf{h}_u^t\right\|^2\right] \\ &\stackrel{(a)}{\leq} \sum_{u=0}^{U-1}\alpha_u\mathbb{E}\left[\left\|\Delta_u^t\nabla f_u(\mathbf{w}^t) - \lambda_u^t\nabla f_u(\mathbf{w}^t) + \lambda_u^t\nabla f_u(\mathbf{w}^t) - \lambda_u^t\mathbf{h}_u^t + \lambda_u^t\mathbf{h}_u^t - \Delta_u^t\mathbf{h}_u^t\right\|^2\right] \\ &= \sum_{u=0}^{U-1}\alpha_u\mathbb{E}\left[\left\|(\Delta_u^t - \lambda_u^t)\nabla f_u(\mathbf{w}^t) + \lambda_u^t(\nabla f_u(\mathbf{w}^t) - \mathbf{h}_u^t) - (\Delta_u^t - \lambda_u^t)\mathbf{h}_u^t\right\|^2\right] \\ &= \sum_{u=0}^{U-1}\alpha_u\mathbb{E}\left[\left\|(\Delta_u^t - \lambda_u^t)[\nabla f_u(\mathbf{w}^t) - \mathbf{h}_u^t] + \lambda_u^t(\nabla f_u(\mathbf{w}^t) - \mathbf{h}_u^t)\right\|^2\right] \\ &\stackrel{(b)}{\leq} 2\sum_{u=0}^{U-1}\alpha_u\mathbb{E}\left[\left\|(\Delta_u^t - \lambda_u^t)[\nabla f_u(\mathbf{w}^t) - \mathbf{h}_u^t]\right\|^2\right] + 2\sum_{u=0}^{U-1}\alpha_u\mathbb{E}\left[\left\|\lambda_u^t(\nabla f_u(\mathbf{w}^t) - \mathbf{h}_u^t)\right\|^2\right] \\ &= 2\sum_{u=0}^{U-1}\alpha_u\left[(\Delta_u^t)^2 - 2\Delta_u^t\lambda_u^t + (\lambda_u^t)^2\right]\mathbb{E}\left[\left\|\nabla f_u(\mathbf{w}^t) - \mathbf{h}_u^t\right\|^2\right] + 2\sum_{u=0}^{U-1}\alpha_u(\lambda_u^t)^2\mathbb{E}\left[\left\|\nabla f_u(\mathbf{w}^t) - \mathbf{h}_u^t\right\|^2\right] \\ &= 2\sum_{u=0}^{U-1}\alpha_u\left[(\Delta_u^t)^2 - 2\Delta_u^t\lambda_u^t + 2(\lambda_u^t)^2\right]\mathbb{E}\left[\left\|\nabla f_u(\mathbf{w}^t) - \frac{1}{\kappa_u^t}\sum_{\tau=0}^{\kappa_u^t-1}\nabla f_u(\mathbf{w}_u^{t,\tau})\right\|^2\right] \\ &= 2\sum_{u=0}^{U-1}\alpha_u\left[(\Delta_u^t)^2 - 2\Delta_u^t\lambda_u^t + 2(\lambda_u^t)^2\right]\mathbb{E}\left[\left\|\frac{1}{\kappa_u^t}\sum_{\tau=0}^{\kappa_u^t-1}\nabla f_u(\mathbf{w}^t) - \frac{1}{\kappa_u^t}\sum_{\tau=0}^{\kappa_u^t-1}\nabla f_u(\mathbf{w}_u^{t,\tau})\right\|^2\right] \\ &= 2\sum_{u=0}^{U-1}\alpha_u\frac{[(\Delta_u^t)^2 - 2\Delta_u^t\lambda_u^t + 2(\lambda_u^t)^2]}{(\kappa_u^t)^2}\mathbb{E}\left[\left\|\sum_{\tau=0}^{\kappa_u^t-1}(\nabla f_u(\mathbf{w}^t) - \nabla f_u(\mathbf{w}_u^{t,\tau}))\right\|^2\right] \\ &\stackrel{(c)}{\leq} 2\sum_{u=0}^{U-1}\alpha_u\frac{[(\Delta_u^t)^2 - 2\Delta_u^t\lambda_u^t + 2(\lambda_u^t)^2]}{\kappa_u^t}\sum_{\tau=0}^{\kappa_u^t-1}\mathbb{E}\left[\left\|\nabla f_u(\mathbf{w}^t) - \nabla f_u(\mathbf{w}_u^{t,\tau})\right\|^2\right] \\ &\stackrel{(d)}{\leq} 2\beta^2\sum_{u=0}^{U-1}\alpha_u\frac{[(\Delta_u^t)^2 - 2\Delta_u^t\lambda_u^t + 2(\lambda_u^t)^2]}{\kappa_u^t}\sum_{\tau=0}^{\kappa_u^t-1}\mathbb{E}\left[\left\|\mathbf{w}^t - \mathbf{w}_u^{t,\tau}\right\|^2\right], \end{aligned} \quad (47)$$

where (a) appears from the convexity of $\|\cdot\|$ and Jensen inequality, i.e., $\|\sum_{i=1}^I\alpha_i\mathbf{x}_i\|^2 \leq \sum_{i=1}^I\alpha_i\|\mathbf{x}_i\|^2$ since $\sum_{i=1}^I\alpha_i = 1$. Besides, (b) and c are the result of the fact $\|\sum_{i=1}^I\mathbf{x}_i\|^2 \leq I\|\mathbf{x}_i\|^2$. Moreover, (d) stems from the β -smoothness assumption.

Plugging T_3 into (46) and dividing both sides by $\frac{\eta\tilde{\eta}}{2}$, we get

$$\begin{aligned} \frac{2(\mathbb{E}[f(\mathbf{w}^{t+1})] - \mathbb{E}[f(\mathbf{w}^t)])}{\eta\tilde{\eta}} &\leq -\mathbb{E}\|\nabla f(\mathbf{w}^t)\|^2 + \beta\eta\tilde{\eta}\sigma^2\sum_{u=0}^{U-1}\alpha_u^2(\Delta_u^t)^2 + \\ &\quad 2\beta^2\sum_{u=0}^{U-1}\alpha_u\frac{[(\Delta_u^t)^2 - 2\Delta_u^t\lambda_u^t + 2(\lambda_u^t)^2]}{\kappa_u^t}\sum_{\tau=0}^{\kappa_u^t-1}\mathbb{E}\left[\left\|\mathbf{w}^t - \mathbf{w}_u^{t,\tau}\right\|^2\right]. \end{aligned} \quad (48)$$

T_4 is further simplified as

$$\begin{aligned} \mathbb{E}\left\|\mathbf{w}^t - \mathbf{w}_u^{t,\tau}\right\|^2 &= \mathbb{E}\left\|\mathbf{w}^t - \mathbf{w}_u^{t,0} + \eta\sum_{\tau'=0}^{\tau-1}g_u(\mathbf{w}_u^{t,\tau'})\right\|^2 \\ &\stackrel{(a)}{=} \eta^2\mathbb{E}\left\|\sum_{\tau'=0}^{\tau-1}g_u(\mathbf{w}_u^{t,\tau'})\right\|^2 \end{aligned}$$

$$\begin{aligned}
&= \eta^2 \mathbb{E} \left\| \sum_{\tau'=0}^{\tau-1} g_u(\mathbf{w}_u^{t,\tau'}) - \sum_{\tau'=0}^{\tau-1} \nabla f_u(\mathbf{w}_u^{t,\tau'}) + \sum_{\tau'=0}^{\tau-1} \nabla f_u(\mathbf{w}_u^{t,\tau'}) \right\|^2 \\
&\stackrel{(b)}{\leq} 2\eta^2 \mathbb{E} \left\| \sum_{\tau'=0}^{\tau-1} g_u(\mathbf{w}_u^{t,\tau'}) - \sum_{\tau'=0}^{\tau-1} \nabla f_u(\mathbf{w}_u^{t,\tau'}) \right\|^2 + 2\eta^2 \mathbb{E} \left\| \sum_{\tau'=0}^{\tau-1} \nabla f_u(\mathbf{w}_u^{t,\tau'}) \right\|^2 \\
&\stackrel{(c)}{\leq} 2\eta^2 \sum_{\tau'=0}^{\tau-1} \mathbb{E} \left\| g_u(\mathbf{w}_u^{t,\tau'}) - \nabla f_u(\mathbf{w}_u^{t,\tau'}) \right\|^2 + 2\kappa_u^t \eta^2 \sum_{\tau'=0}^{\tau-1} \mathbb{E} \left\| \nabla f_u(\mathbf{w}_u^{t,\tau'}) \right\|^2 \\
&\stackrel{(d)}{\leq} 2\eta^2 \sum_{\tau'=0}^{\tau-1} \sigma^2 + 2\eta^2 (\kappa_u^t)^2 \mathbb{E} \left\| \nabla f_u(\mathbf{w}_u^{t,\tau}) \right\|^2 \\
&\stackrel{(e)}{\leq} 2\kappa_u^t \eta^2 \sigma^2 + 2\eta^2 (\kappa_u^t)^2 \mathbb{E} \left\| \nabla f_u(\mathbf{w}_u^{t,\tau}) \right\|^2 \\
&= 2\kappa_u^t \eta^2 \sigma^2 + 2\eta^2 (\kappa_u^t)^2 \mathbb{E} \left[\left\| \nabla f_u(\mathbf{w}_u^{t,\tau}) - \nabla f_u(\mathbf{w}^t) + \nabla f_u(\mathbf{w}^t) - \nabla f(\mathbf{w}^t) + \nabla f(\mathbf{w}^t) \right\|^2 \right] \\
&\stackrel{(f)}{\leq} 2\kappa_u^t \eta^2 \sigma^2 + 6\eta^2 (\kappa_u^t)^2 \mathbb{E} \left[\left\| \nabla f_u(\mathbf{w}_u^{t,\tau}) - \nabla f_u(\mathbf{w}^t) \right\|^2 + \mathbb{E} \left\| \nabla f_u(\mathbf{w}^t) - \nabla f(\mathbf{w}^t) \right\|^2 + \mathbb{E} \left\| \nabla f(\mathbf{w}^t) \right\|^2 \right] \\
&\stackrel{(g)}{\leq} 2\kappa_u^t \eta^2 \sigma^2 + 6\eta^2 (\kappa_u^t)^2 \varepsilon^2 + 6\beta^2 \eta^2 (\kappa_u^t)^2 \mathbb{E} \left[\left\| \mathbf{w}_u^{t,\tau} - \mathbf{w}^t \right\|^2 \right] + 6\eta^2 (\kappa_u^t)^2 \mathbb{E} \left[\left\| \nabla f(\mathbf{w}^t) \right\|^2 \right] \\
&\stackrel{(h)}{\leq} 2\kappa_u^t \eta^2 \sigma^2 + 6\eta^2 (\kappa_u^t)^2 \varepsilon^2 + 6\beta^2 \eta^2 (\kappa_u^t)^2 \mathbb{E} \left[\left\| \mathbf{w}_u^{t,\tau} - \mathbf{w}^t \right\|^2 \right] + 6\eta^2 \kappa^2 \mathbb{E} \left[\left\| \nabla f(\mathbf{w}^t) \right\|^2 \right] \tag{49}
\end{aligned}$$

where (a) comes from the fact that $\mathbf{w}_u^{t,0} \leftarrow \mathbf{w}^t$ during the synchronization. Besides, (b) appears from the fact $\|\sum_{i=1}^I \mathbf{x}_i\|^2 \leq I\|\mathbf{x}_i\|^2$. The first in (c) is the result of the unbiased stochastic gradients assumption and independence of the stochastic gradients. Furthermore, we use the facts $\|\sum_{i=1}^I \mathbf{x}_i\|^2 \leq I\|\mathbf{x}_i\|^2$ and $0 \leq [(\tau-1) - \tau'] \leq \kappa_u^t$ to get the second term in (c). We use the bounded variance of the stochastic gradient assumption in (d), while (e) is true since $0 \leq [(\tau-1) - \tau'] \leq \kappa_u^t$. (f) comes from the same fact as in (b). Moreover, (g) stems from the β -Lipschitz smoothness assumption. Finally, (h) comes from the fact that $1 \leq \kappa_u^t \leq \kappa$.

Rearranging the terms, we can write

$$\mathbb{E} \left\| \mathbf{w}^t - \mathbf{w}_u^{t,\tau} \right\|^2 \leq \frac{2\kappa_u^t \eta^2 \sigma^2 + 6\eta^2 (\kappa_u^t)^2 \varepsilon^2 + 6\eta^2 \kappa^2 \mathbb{E} \left[\left\| \nabla f(\mathbf{w}^t) \right\|^2 \right]}{1 - 6\beta^2 \eta^2 (\kappa_u^t)^2}. \tag{50}$$

When $\eta < \frac{1}{\sqrt{6\beta\kappa_u^t}}$, we have $0 < (1 - 6\beta^2 \eta^2 (\kappa_u^t)^2) < 1$. Moreover, since $1 \leq \kappa_u^t \leq \kappa$, the above condition is always satisfied if $\eta \leq \frac{1}{\sqrt{6\beta\kappa}}$. As such, we approximate T_4 as follows:

$$\mathbb{E} \left\| \mathbf{w}^t - \mathbf{w}_u^{t,\tau} \right\|^2 \leq 2\kappa_u^t \eta^2 \sigma^2 + 6\eta^2 (\kappa_u^t)^2 \varepsilon^2 + 6\eta^2 \kappa^2 \mathbb{E} \left[\left\| \nabla f(\mathbf{w}^t) \right\|^2 \right]. \tag{51}$$

Now, plugging T_4 into (48), we get

$$\begin{aligned}
&\frac{2(\mathbb{E}[f(\mathbf{w}^{t+1})] - \mathbb{E}[f(\mathbf{w}^t)])}{\eta \tilde{\eta}} \leq -\mathbb{E} \left\| \nabla f(\mathbf{w}^t) \right\|^2 + \beta \eta \tilde{\eta} \sigma^2 \sum_{u=0}^{U-1} \alpha_u^2 (\Delta_u^t)^2 + \\
&\quad 2\beta^2 \sum_{u=0}^{U-1} \alpha_u \frac{[(\Delta_u^t)^2 - 2\Delta_u^t \lambda_u^t + 2(\lambda_u^t)^2]}{\kappa_u^t} \sum_{\tau=0}^{\kappa_u^t-1} \left[2\kappa_u^t \eta^2 \sigma^2 + 6\eta^2 (\kappa_u^t)^2 \varepsilon^2 + 6\eta^2 \kappa^2 \mathbb{E} \left[\left\| \nabla f(\mathbf{w}^t) \right\|^2 \right] \right] \\
&= -\mathbb{E} \left\| \nabla f(\mathbf{w}^t) \right\|^2 + \beta \eta \tilde{\eta} \sigma^2 \sum_{u=0}^{U-1} \alpha_u^2 (\Delta_u^t)^2 + \\
&\quad 2\beta^2 \sum_{u=0}^{U-1} \alpha_u \frac{[(\Delta_u^t)^2 - 2\Delta_u^t \lambda_u^t + 2(\lambda_u^t)^2]}{\kappa_u^t} \times \kappa_u^t \left[2\kappa_u^t \eta^2 \sigma^2 + 6\eta^2 (\kappa_u^t)^2 \varepsilon^2 + 6\eta^2 \kappa^2 \mathbb{E} \left[\left\| \nabla f(\mathbf{w}^t) \right\|^2 \right] \right] \\
&= \left[12\beta^2 \eta^2 \kappa^2 \sum_{u=0}^{U-1} \alpha_u [(\Delta_u^t)^2 - 2\Delta_u^t \lambda_u^t + 2(\lambda_u^t)^2] - 1 \right] \mathbb{E} \left\| \nabla f(\mathbf{w}^t) \right\|^2 + \beta \eta \tilde{\eta} \sigma^2 \sum_{u=0}^{U-1} \alpha_u^2 (\Delta_u^t)^2 + \\
&\quad 4\beta^2 \eta^2 \sigma^2 \sum_{u=0}^{U-1} \alpha_u \kappa_u^t [(\Delta_u^t)^2 - 2\Delta_u^t \lambda_u^t + 2(\lambda_u^t)^2] + 12\beta^2 \eta^2 \varepsilon^2 \sum_{u=0}^{U-1} \alpha_u [(\Delta_u^t)^2 - 2\Delta_u^t \lambda_u^t + 2(\lambda_u^t)^2] (\kappa_u^t)^2, \tag{52}
\end{aligned}$$

Rearranging the terms, we write

$$\begin{aligned}
\mathbb{E} \left\| \nabla f(\mathbf{w}^t) \right\|^2 \leq &\frac{1}{1 - 12\beta^2 \eta^2 \kappa^2 \sum_{u=0}^{U-1} \alpha_u [(\Delta_u^t)^2 - 2\Delta_u^t \lambda_u^t + 2(\lambda_u^t)^2]} \left[\frac{2(\mathbb{E}[f(\mathbf{w}^t)] - \mathbb{E}[f(\mathbf{w}^{t+1})])}{\eta \tilde{\eta}} + \beta \eta \tilde{\eta} \sigma^2 \sum_{u=0}^{U-1} \alpha_u^2 (\Delta_u^t)^2 + \right. \\
&\left. 4\beta^2 \eta^2 \sigma^2 \sum_{u=0}^{U-1} \alpha_u \kappa_u^t [(\Delta_u^t)^2 - 2\Delta_u^t \lambda_u^t + 2(\lambda_u^t)^2] + 12\beta^2 \eta^2 \varepsilon^2 \sum_{u=0}^{U-1} \alpha_u [(\Delta_u^t)^2 - 2\Delta_u^t \lambda_u^t + 2(\lambda_u^t)^2] (\kappa_u^t)^2 \right]. \tag{53}
\end{aligned}$$

Averaging over time gives

$$\begin{aligned}
\frac{1}{T} \sum_{t=0}^{T-1} \mathbb{E} \|\nabla f(\mathbf{w}^t)\|^2 &\leq \frac{1}{T} \sum_{t=0}^{T-1} \left\{ \frac{1}{1 - 12\beta^2\eta^2\kappa^2 \sum_{u=0}^{U-1} \alpha_u [(\Delta_u^t)^2 - 2\Delta_u^t\lambda_u^t + 2(\lambda_u^t)^2]} \left[\frac{2(\mathbb{E}[f(\mathbf{w}^t)] - \mathbb{E}[f(\mathbf{w}^{t+1})])}{\eta\tilde{\eta}} + \right. \right. \\
&\quad \beta\eta\tilde{\eta}\sigma^2 \sum_{u=0}^{U-1} \alpha_u^2 (\Delta_u^t)^2 + 4\beta^2\eta^2\sigma^2 \sum_{u=0}^{U-1} \alpha_u \kappa_u^t [(\Delta_u^t)^2 - 2\Delta_u^t\lambda_u^t + 2(\lambda_u^t)^2] + \\
&\quad \left. \left. 12\beta^2\eta^2\varepsilon^2 \sum_{u=0}^{U-1} \alpha_u [(\Delta_u^t)^2 - 2\Delta_u^t\lambda_u^t + 2(\lambda_u^t)^2] (\kappa_u^t)^2 \right] \right\}. \tag{54}
\end{aligned}$$

■